Article

Cell

Clonal Evolution of Autoreactive Germinal Centers

Graphical Abstract

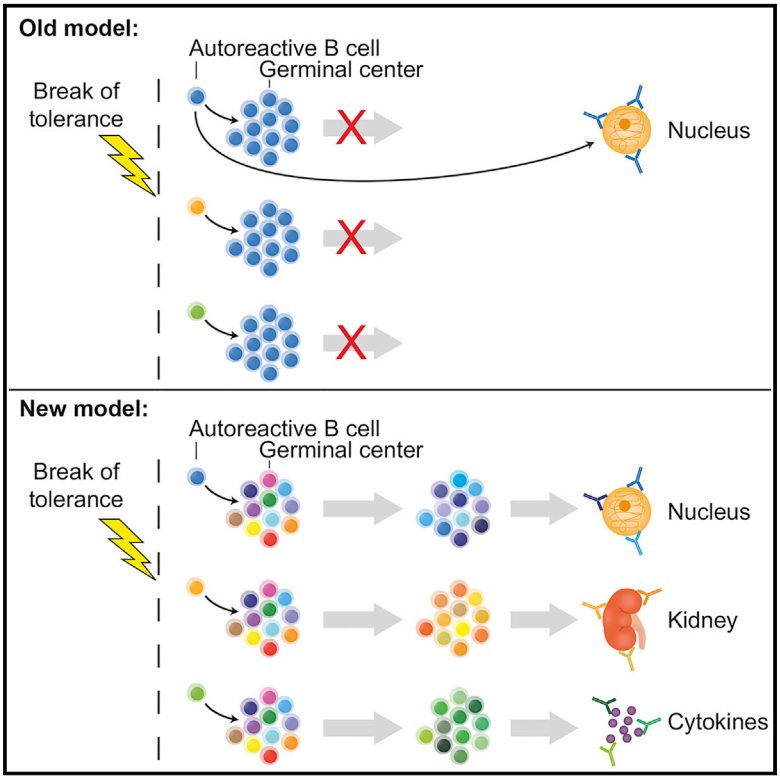

Highlights

- Single autoreactive B cell clone drives expansion of WT B cells in germinal centers
- Autoreactive germinal centers composed of WT B cells become self-sufficient
- Autoreactive and foreign antigen germinal centers evolve clonally at similar rates
- Clonal expansion of WT B cells in germinal centers underlies epitope spreading

Authors

Søren E. Degn, Cees E. van der Poel, Daniel J. Firl, ..., Paul J. Utz, Gabriel D. Victora, Michael C. Carroll

Correspondence

sdegn@biomed.au.dk (S.E.D.), michael.carroll@childrens.harvard.edu (M.C.C.)

In Brief

Following the natural history of autoreactive germinal centers in vivo opens a window into how self-tolerance is broken in lupus and other complex autoimmune diseases.

Degn et al., 2017, Cell *170*, 913–926
August 24, 2017
http://dx.doi.org/10.1016/j.cell.2017.07.026

CellPress

Cell

Clonal Evolution of Autoreactive Germinal Centers

Søren E. Degn,[1,2,*] Cees E. van der Poel,[1] Daniel J. Firl,[1,3] Burcu Ayoglu,[4] Fahd A. Al Qureshah,[1,5] Goran Bajic,[6] Luka Mesin,[7,9] Claude-Agnès Reynaud,[8] Jean-Claude Weill,[8] Paul J. Utz,[4] Gabriel D. Victora,[7,9] and Michael C. Carroll[1,10,*]
[1]Program in Cellular and Molecular Medicine, Boston Children's Hospital, Harvard Medical School, Boston, MA 02115, USA
[2]Department of Biomedicine, Aarhus University, 8000 Aarhus C, Denmark
[3]Howard Hughes Medical Institute, Chevy Chase, MD 20815, USA
[4]Department of Medicine, Stanford University, Stanford, CA 94305, USA
[5]King Abdulaziz City for Science and Technology, Riyadh 11442, Saudi Arabia
[6]Laboratory of Molecular Medicine, Boston Children's Hospital, Harvard Medical School, Boston, MA 02115, USA
[7]Whitehead Institute for Biomedical Research, Cambridge, MA 02142, USA
[8]Institut Necker Enfants Malades, INSERM U1151/CNRS UMS 8253, Université Paris Descartes, Sorbonne Paris Cité, 75993 Paris Cedex 14, France
[9]Present address: The Rockefeller University, New York, NY 10065, USA
[10]Lead Contact
*Correspondence: sdegn@biomed.au.dk (S.E.D.), michael.carroll@childrens.harvard.edu (M.C.C.)
http://dx.doi.org/10.1016/j.cell.2017.07.026

SUMMARY

Germinal centers (GCs) are the primary sites of clonal B cell expansion and affinity maturation, directing the production of high-affinity antibodies. This response is a central driver of pathogenesis in autoimmune diseases, such as systemic lupus erythematosus (SLE), but the natural history of autoreactive GCs remains unclear. Here, we present a novel mouse model where the presence of a single autoreactive B cell clone drives the TLR7-dependent activation, expansion, and differentiation of other autoreactive B cells in spontaneous GCs. Once tolerance was broken for one self-antigen, autoreactive GCs generated B cells targeting other self-antigens. GCs became independent of the initial clone and evolved toward dominance of individual clonal lineages, indicating affinity maturation. This process produced serum autoantibodies to a breadth of self-antigens, leading to antibody deposition in the kidneys. Our data provide insight into the maturation of the self-reactive B cell response, contextualizing the epitope spreading observed in autoimmune disease.

INTRODUCTION

Systemic lupus erythematosus (SLE) is characterized by the production of antibodies to nucleic acid antigens (Ags) (Rahman and Isenberg, 2008), with >75% of patients having serum autoantibodies to double-stranded DNA (compared to ~0.5% of healthy controls), which typically appear a few years before SLE is diagnosed (Arbuckle et al., 2003). SLE patients at or after disease onset drift in their serological reactivities toward a variety of nuclear, nucleolar, and protein-DNA complexes: a process known as epitope spreading. Although the mechanism is not well understood, epitope spreading is thought to be driven by chronic immune responses causing inclusion of new autoreactive B cell clones (Arbuckle et al., 2003; Cornaby et al., 2015; Vanderlugt and Miller, 2002).

Affinity-matured antibodies (Abs) arise in germinal centers (GCs), wherein B cell clones cycle between division, somatic hypermutation (SHM) and selection based on Ag affinity (Victora et al., 2010). This process of random mutation can generate BCRs that recognize self-Ags (Mietzner et al., 2008; Tiller et al., 2007); however, it has long been thought that GCs are able to limit the affinity maturation of autoreactive cells (Han et al., 1995; Pulendran et al., 1995; Shokat and Goodnow, 1995; Vinuesa et al., 2009). In fact, display of self-Ag by follicular dendritic cells (FDCs) within GCs can delete autoreactive cells (Yau et al., 2013), and autoreactive B cells can mutate away from autoreactivity (Reed et al., 2016; Sabouri et al., 2014). Therefore, it has remained questionable whether autoreactive B cells in GCs follow the same rules of Ag engagement with FDCs, clonal evolution, and affinity maturation as those in foreign-Ag-elicited GCs.

Many autoimmune mouse models have spontaneous GC formation (Luzina et al., 2001), but as these models are based on genetically modified B or T cells or have uncharacterized, complex genetic backgrounds, they are poorly suited to studying natural autoreactive GC behavior. Here, we developed a chimera mouse model that has spontaneous autoreactive GCs composed of self-reactive B cells from the wild-type (WT) repertoire in a genetically normal context. Surprisingly, we find that there is no limit on the evolution of autoreactive GCs—that is, they generate B cells targeting other self-Ags once tolerance is broken.

RESULTS

564Igi Mice Display Spontaneous GCs, VDJ Diversification, SHM, and CSR

The 564Igi mouse is a murine model of SLE on C57BL/6 (B6) background, generated by knock in of the heavy (H) and kappa light (K) chain of an autoreactive B cell clone targeting ribonuclear complexes (Berland et al., 2006). In heterozygous 564Igi

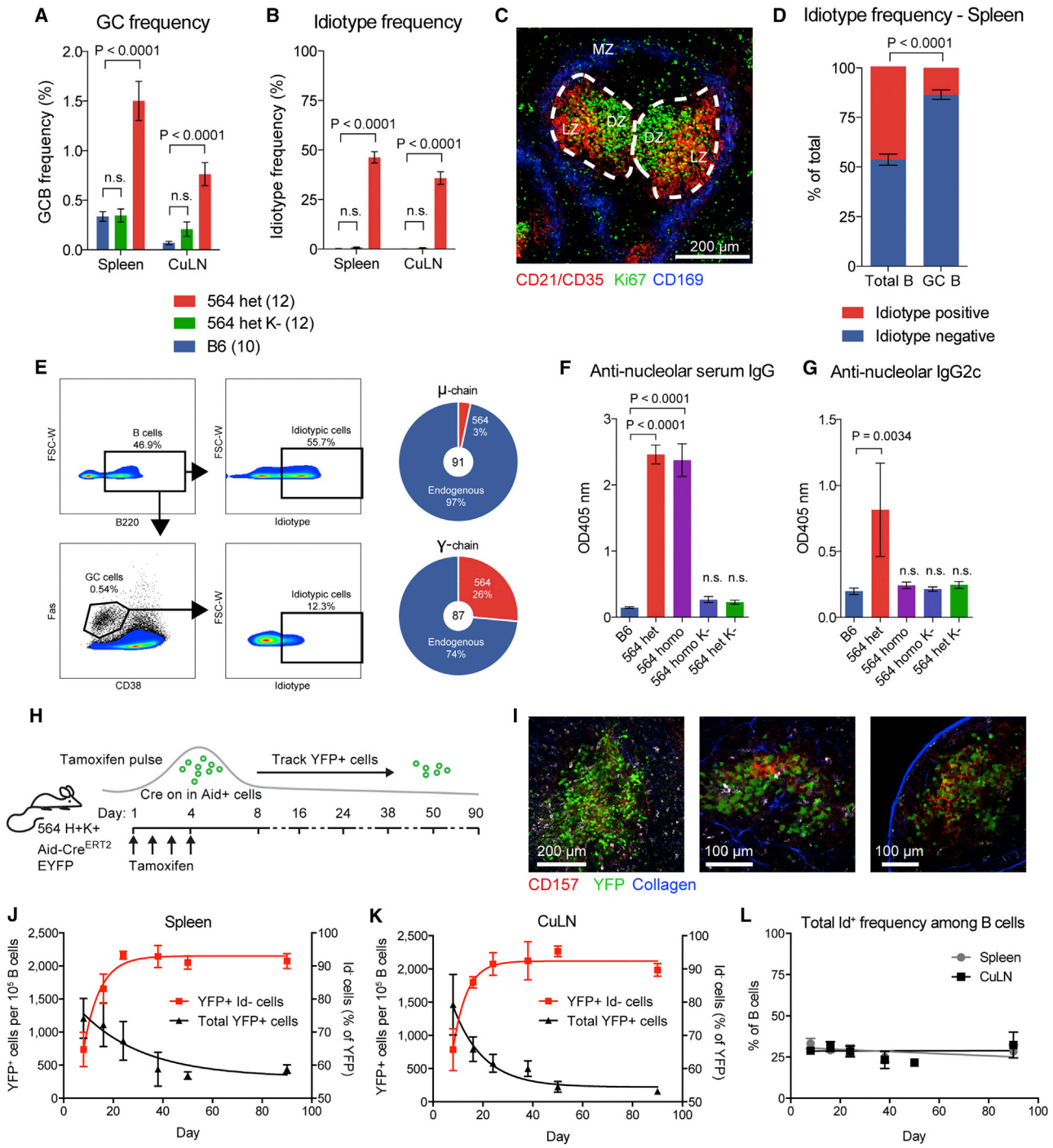

Figure 1. Spontaneous, Chronic GCs in 564Igi Mice Display VDJ Diversification, SHM, and CSR

(A) GC frequency within the B220$^+$ gate of B6 (n = 10), heterozygous 564Igi K$^-$ (n = 12), and heterozygous 564Igi mice (n = 12). Mean ± SEM, multiplicity-adjusted p values for two-way ANOVA with Dunnett's posttest.

(B) Id frequency within the B220$^+$ gate as in (A).

(C) Representative confocal immunofluorescence (IF) microscopy of a 10-µm splenic section from a heterozygous 564Igi mouse, displaying GC structures identified by staining for CD21/35 (dim on B cells, bright on FDC in the light zone [LZ], red) and centroblasts (dividing cells in the dark zone [DZ], Ki67-positive cells, green), and staining of the marginal zone (MZ, CD169$^+$ metallophilic macrophages, blue) indicating the border of the red and white pulp.

(D) Frequency of Id$^+$ versus Id$^-$ cells in the total versus GC B cell gate in spleen for the group of mice represented in (A) and (B). Mean ± SEM, multiplicity-adjusted p value for repeated-measures two-way ANOVA with Sidak's posttest.

(legend continued on next page)

mice, which carry a single copy of the knockin H and K chain, ~50% of circulating B cells express the knockin BCR (identified by anti-idiotype [Id] Ab staining). The remaining half are Id negative (Id^-) due to receptor editing or allelic inclusion (Berland et al., 2006; Chatterjee et al., 2013; Das et al., 2017; Luning Prak et al., 2011). The mice have high titers of IgG against nuclear-associated Ags, but do not exhibit disease until late in life.

Already at 6 weeks of age, heterozygous 564Igi mice (564het) harbored robust GC B cell populations in spleen and cutaneous lymph nodes (LN) (Figure 1A). Littermates that had the H chain knockin but lacked the K chain (564het K^-) had baseline GC B cell frequencies comparable to B6 controls (Figure 1A). The presence of spontaneous GC B cells correlated with the presence of circulating Id^+ (knockin BCR) cells (Figures 1B and S1A, Spearman correlation, $p = 0.0002$ and $p < 0.0001$, for spleen and LN, respectively). As reported previously, GC structures were found in the spleens of heterozygous 564Igi mice (Chatterjee et al., 2013) (Figure 1C).

Strikingly, Id^+ cells were underrepresented in GCs compared to the circulating repertoire (Figure 1D). GC B cells were sorted from the spleens of two heterozygous 564Igi mice, and sequencing their BCR repertoire revealed that ~95% of the IgM and ~75% of the IgG sequences were not derived from the knockin allele (Figure 1E; Table S1) but were derived by V(D)J recombination of the other allele or by receptor editing of the knockin allele (essentially recombining it again). These "WT-derived B cells" had undergone SHM, as judged by the mutations in their heavy chain VDJ (Figure S1B), and the mutation frequency was higher in IgG sequences than in IgM sequences (two-tailed Mann-Whitney test, $p < 0.0001$), suggesting affinity maturation and class-switch recombination (CSR), but it was unclear whether these WT-derived clones were autoreactive.

We next assessed the reactivity of WT-derived serum antibodies to nucleolar autoAg. The 564Igi heavy chain locus is derived from the IgH-1a allotype (that encodes IgG2a), whereas the endogenous B6 heavy chain locus is IgH-1b (that encodes IgG2c). Therefore, we can distinguish antibodies produced by 564Igi B cells versus WT based on their respective IgG2a and IgG2c allotypes. We screened for IgG2c antibodies against nucleolar autoAg in the sera of heterozygous 564Igi mice. Samples from B6 (IgG2c only), heterozygous 564Igi kappa negative (564het K^-) (IgG2a and IgG2c), and homozygous 564Igi (IgG2a only) mice were included as controls. As expected, heterozygous and homozygous 564Igi mice harbored IgG antibodies targeting nucleoli, whereas B6 and 564het K^- littermates did not (Figure 1F). Strikingly, heterozygous 564Igi mice harbored IgG2c Ab targeting nucleoli (Figure 1G), meaning that a subset of their WT-derived B cells had become autoreactive.

To investigate the trajectory of Id frequencies in spontaneous GCs, the 564Igi strain was crossed to an Aid-Cre^{ERT2} EYFP reporter (Dogan et al., 2009). In this model, GC B cells will constitutively express YFP upon tamoxifen administration, allowing us to track these cells and their progeny (Figure 1H). Following tamoxifen injection, YFP^+ cells represented 2/3 to 3/4 of the total GC B cell population (day 8, ~1,500 YFP^+ cells per 10^5 B cells, with most YFP^+ cells being GC B cells, compared with a total GC B cell frequency of ~2,000 per 10^5) (Figures 1I–1K and S1C; Movies S1 and S2). The fidelity and tamoxifen dependence of the YFP expression were verified in control experiments (Figures S1D–S1J).

The YFP^+ GC population and its progeny were followed for 3 months, showing an overall steady decrease in YFP^+ cells with an increase in Id^- YFP^+ cells (Figures 1J and 1K), despite circulating Id frequencies remaining constant (Figure 1L). Bulk sorting and sequencing of YFP^+ cells 90 days after tamoxifen revealed that >80% of IgM sequences and >90% of IgG sequences were not derived from the 564 knockin allele (Figure S1K), confirming that high numbers of WT-derived B cells were included in the GC and downstream plasma and memory cell population over time. These cells had undergone SHM, with more mutations in IgG sequences than in IgM sequences (two-tailed Mann-Whitney test, $p < 0.0001$; Figure S1L), supporting affinity maturation and CSR. SHM is classically associated with GC responses, but also occurs in extrafollicular foci (Herlands et al., 2008; William et al., 2002). However, the observed mutation rates of the YFP cells were an order of magnitude above those expected from extrafollicular foci. Taken together, these results demonstrate that in heterozygous 564Igi mice, autoreactive WT-derived cells are maturing in spontaneous GCs, thus undergoing affinity maturation, SHM, and CSR.

564Igi Mixed Chimeras Have Spontaneous GCs Composed of WT B Cells

In heterozygous 564Igi mice, spontaneous GCs were predominantly composed of GC B cells with WT-derived BCRs. However, all developing B cells in these mice harbor the knockin allele, thus they are not strictly WT B cells. To follow true WT cells in spontaneous GCs, we used a mixed chimera approach. WT B6 mice were irradiated, ablating their immune system, and reconstituted with a mixture of bone marrows (BM) from WT

(E) Fluorescence-activated cell sorting (FACS) plots showing frequency of Id^+ cells within the total $B220^+$ pool (top right) versus the GC population (bottom right) defined as Fas^+CD38^- B cells. Sequencing of the mu chain (top) and gamma chain (bottom) of FACS-sorted GC B cells of heterozygous 564Igi mice.

(F) Anti-nucleolar serum IgG of B6 (n = 4), heterozygous 564Igi (n = 10), homozygous 564Igi (n = 7), heterozygous 564Igi K^- (n = 8), and homozygous 564Igi K^- mice (n = 3), as measured by ELISA. Mean ± SEM, multiplicity-adjusted p values for one-way ANOVA with Dunnett's posttest.

(G) Anti-nucleolar serum IgG2c as in (F).

(H) Overview of experimental approach.

(I) Representative two-photon imaging of explanted spleen at low (left) and high (middle) magnification, and of explanted inguinal LN at high magnification (right), showing YFP^+ cells (green), $CD157^+$ FDC (red), and second harmonics generation (blue).

(J) A pulsed GC population followed in the spleen over 90 days. Mean ± SEM for 6 (day 8, 16, 24), 2 (day 38 and 50), and 3 (day 90) mice from 3 independent cohorts.

(K) Similar to (J), but for cutaneous LN.

(L) Overall Id frequencies in spleen and LN over the course of the experiment.

See also Figure S1 and Movies S1 and S2.

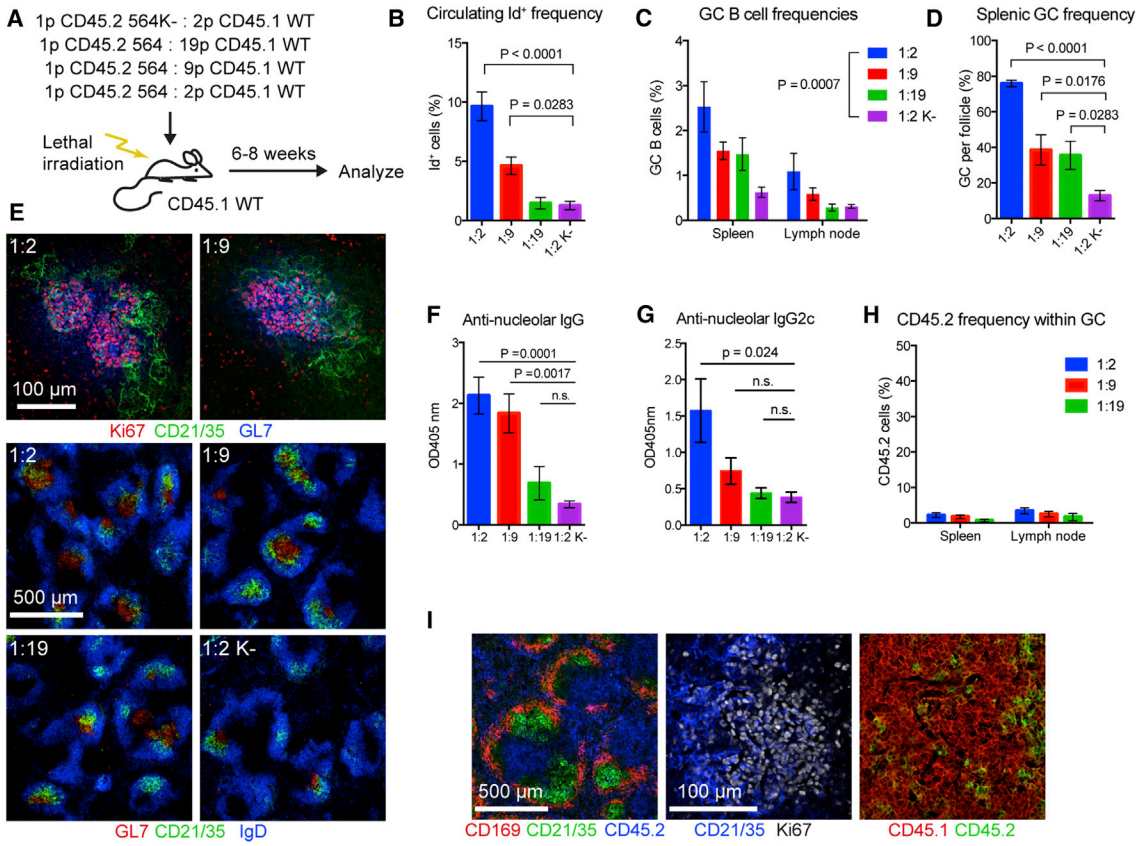

Figure 2. An Autoreactive B Cell Clone Is Sufficient to Induce Spontaneous GCs Composed Predominantly of WT-Derived B Cells

(A) Overview of experimental approach for generating and analyzing 564 CD45.1 mixed chimeras.

(B) Id frequencies in chimera blood. Mean ± SEM for 1:2 (n = 7), 1:9 (n = 7), 1:19 (n = 5), and 1:2K^{-} (n = 5) chimeras from 3 independent cohorts. Multiplicity-adjusted p value for one-way ANOVA using Holm-Sidak's posttest.

(C) GC B cell frequencies in spleen and cutaneous LN analyzed by flow cytometry. As for (B), but using two-way ANOVA with Holm-Sidak's posttest.

(D) Frequency of GC per follicle assessed by confocal IF microscopy. Two slices per mouse listed in (B). Mean ± SEM, multiplicity-adjusted p value for one-way ANOVA using Holm-Sidak's posttest.

(E) Representative confocal IF microscopy of 10-µm spleen sections. Top: representative spleen sections showing T-dependent GC defined by GL7 (blue) and Ki67 (red) bounded by FDC networks (green). Bottom: representative spleen sections at lower magnification showing GL7^{+} GC (red) and FDC networks (green) within follicular areas containing IgD-positive B cells (blue).

(F) Serum anti-nucleolar IgG titers for a subset of mice in (B). Mean ± SEM for 1:2 (n = 6), 1:9 (n = 4), 1:19 (n = 5), and 1:2K^{-} (n = 6) chimeras from 3 independent cohorts. Multiplicity-adjusted p value for one-way ANOVA using Holm-Sidak's posttest.

(G) Serum anti-nucleolar IgG2c titers as in (F).

(H) CD45.2 frequencies within GC of (C).

(I) Left: confocal IF microscopy of spleen section showing distribution of 564 BM-derived cells (CD45.2, blue) in relation to the marginal zone (CD169, red) and FDC networks (CD21/35, green). Middle and right: distribution of CD45.2 (green) versus CD45.1 (red) cell populations within the GC defined by FDC (light zone, CD21/35 in blue) and dividing centroblasts (dark zone, Ki67 in white).

See also Figure S2.

B6 and homozygous 564Igi donors. In this scenario, the 564Igi cells still kick-start autoimmunity, but they are "locked in," as they are bi-allelically pre-rearranged, and they are genetically segregated from the WT B cell response (Figure S2A). The cells were followed using two allotypes of leukocyte marker CD45 (CD45.1 for WT cells and CD45.2 for 564Igi cells) (Figure 2A). For controls, we used mixed chimeras in which homozygous 564Igi donors were K-chain negative (CD45.2 564K^{-}) (Figure 2A). T cells should be unaffected by the knockin status, as they do not express the BCR, and all chimeras had the predicted ratios of CD45.1 to CD45.2 T cells.

The mixed chimeras had fewer-than-expected 564Igi B cells (CD45.2) when compared to 564Igi T cells, likely because the autoreactive 564Igi cells were selected against (Figures S2B–S2E). A smaller, but significant negative selection was observed in the BM of 564K^{-} mixed chimeras, likely because of higher tonic BCR signal in the double-heavy-chain-expressing 564K^{-} B cells (Figure S2B). However, in spleen, skin-draining LN, and blood, the reduced frequency of 564Igi B cells was more drastic than for 564K^{-} B cells (Figures S2C–S2E). This finding agrees with the previously reported negative selection of self-reactive B cells at the transitional stage observed in 564Igi mice (Berland et al.,

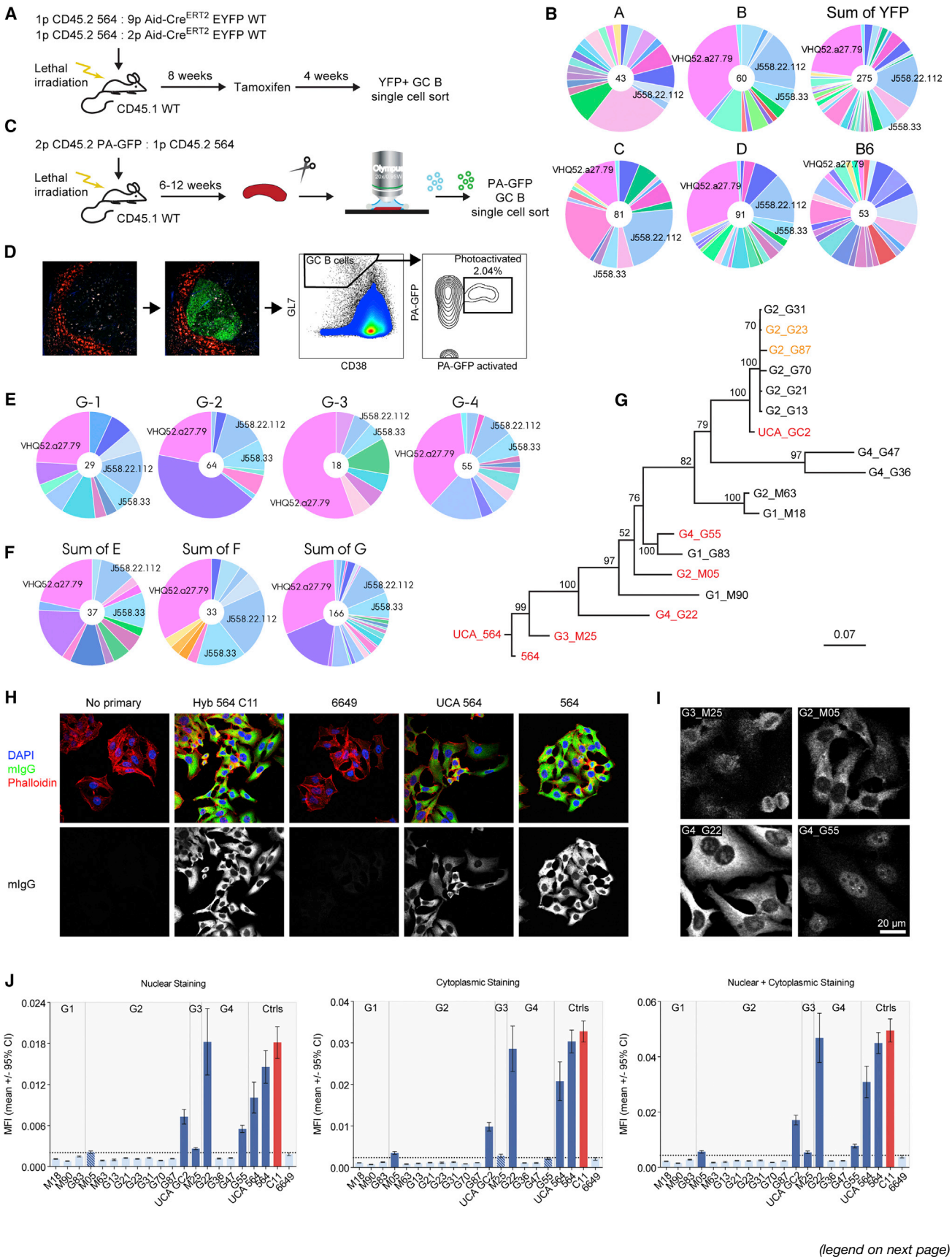

(legend on next page)

2006; Chatterjee et al., 2013). The chimeras displayed normal and consistent total B cell frequency (Figures S2F–S2I).

Despite negative selection against 564Igi B cells, the input BM ratios had a titration effect on circulating Id frequencies (Figure 2B). Weaker effects on GCs were also observed in spleen and skin-draining LN (Figures 2C–2E). The frequency of Id^+ cells in blood correlated with GC B cell frequencies in spleen (Spearman $r = 0.73$, $p < 0.0001$) and skin-draining LN (Spearman $r = 0.65$, $p = 0.0006$) (Figure S2J). Furthermore, the ratios impacted the level of circulating anti-nucleolar IgG and IgG2c (produced by WT cells) (Figures 2F and 2G). Strikingly, at 6–8 weeks post reconstitution, GCs were almost exclusively composed of WT-derived cells (Figures 2H and 2I), while the $564K^-$ chimera controls had no GCs. Because the observed phenotypes were most robust in the 1:2 chimeras, this BM ratio was chosen for most subsequent experiments.

B Cells of Spontaneous GCs in 564Igi Mixed Chimeras Are Autoreactive and Converge on Similar BCRs

To analyze the WT-derived GC B cells further, mixed chimeras were generated using a mixture of BM from Aid-Cre^{ERT2} EYFP WT and homozygous 564Igi donors transferred into irradiated WT recipients (Figure 3A). Following reconstitution, mice were pulsed with tamoxifen, and 4 weeks later, the BCR repertoire of the YFP^+ GC B cells was sequenced (Figures 3A and 3B), capturing a total of 275 heavy chains from 4 chimeras, representing a total of 46 distinct V segments (the V segment determines most of the Ag specificity). The most prevalent V segment accounted for over 1/5 of the total sequences, while the second- and third-most accounted for ~1/6 and ~1/15, respectively. The most prevalent and the second-most prevalent V segment were observed in 3 and 4 out of 4 mice, respectively (Figure 3B), indicating that the WT-derived GC B cells converged on particular heavy chain V segments, suggesting they were targeting similar Ags. The sequences had many mutations, indicating a significant degree of SHM, as compared to naive mature B cells from B6 mice (Kruskal-Wallis test with Dunn's multiple comparison, $p < 0.0001$ for pairwise comparison of mouse A-D with B6) (Figure S3C).

This analysis is a gross under-sampling of a vast pool of B cells and may not adequately reflect clonal selection processes at the level of a single GC. To improve the analysis, chimeras were generated based on mixing WT PA-GFP BM with homozygous 564Igi BM in WT recipients (Figure 3C). Following reconstitution, single GCs from fresh spleen explants were photoactivated as previously described (Victora et al., 2010) and sorted into single cells (Figures 3C and 3D). Again, clonal expansion and selection were observed in the heavy-chain-derived V segments (Figures 3E, 3F, S3A, and S3B). Specifically, the VHQ52.a27.79 (IGHV2-9*02) and J558.33 (IGHV1S81*02) segments occurred in 3/4, 4/4, and 4/4 GCs analyzed in 3 independent chimeras (Figure S3B). Surprisingly, these sequence elements were shared, not only among clones of distinct GC within the same mice, but also among clones of different mice. Again, mutation analysis indicated a significant degree of SHM, both when comparing all sequences from each PA-GFP mouse to naive mature B cells from B6 mice (Kruskal-Wallis test with Dunn's multiple comparison, $p < 0.0001$ for pairwise comparison of E-G with B6) (Figure S3D) and when comparing sequences of individual GC with those from B6 (Kruskal-Wallis test with Dunn's multiple comparison, $p \leq 0.0001$ for pairwise comparison of G1–G4 with B6) (Figure S3E).

Of note, the observed V segments were also prominent in Aid-Cre^{ERT2} EYFP chimeras. Furthermore, we identified similar sequences in YFP^+ cells from tamoxifen-pulsed Aid-Cre^{ERT2} EYFP heterozygous 564Igi mice, indicating that this convergence across independent animals was not an artifact of the chimera approach. An unbiased BLASTP search of CDR3 amino acid

Figure 3. WT GC Cells Converge on Stereotypic Autoreactive Sequence Elements

(A) Overview of experimental setup for single-cell sequence analysis of temporal global GC populations.

(B) Single-cell sequence analysis of temporal global GC populations from 4 mice (two 1:9 [A+B] and two 1:2 chimeras [C+D]), the sum of all observed YFP-derived sequences (from A–D) and a control B6. A unique color is assigned to each unique V element, and colors are consistent across graphs in Figure 3 and Figure S3.

(C) Schematic overview of experimental setup for single GC-level single GC B cell analysis.

(D) Example of photoactivation and sort gates for single GC-level single GC B cell sorting. Leftmost panel: the marginal zone is labeled with anti-CD169-PE and, based on tingible-body macrophage morphology, follicles containing GC are delineated for photoactivation. Second panel from left: GFP signal following photoactivation. Second panel from right: GC B cell gate defined as $CD38^{lo}$, $GL7^{hi}$. Rightmost panel: signal for photoactivated GFP versus unactivated PA-GFP and indication of terminal sort gate for photoactivated GC B cells.

(E) Clonal composition of four splenic GC from the same mouse, as defined by heavy chain V-segments.

(F) Sum of observed Vh segments in four splenic GC each for 3 independent mice.

(G) Phylogenetic tree for the 17 synthesized PA-GFP clones, 564, and the 564 UCA, based on the nucleotide sequences of heavy + light chains. Clones identified as autoreactive in HEp-2 assay, nucleolar ELISA, and autoAg array are highlighted in red, whereas clones displaying limited autoreactivity in autoAg array only are in orange. The tree was resampled 100 times, and the resulting confidence of branchpoint determination is indicated.

(H) Representative results for confocal analysis of human epithelial (HEp-2) cells stained with (from left to right): no primary, 564 Ab derived from a hybridoma (clone C11), cloned heavy and light chain pairs from control anti-influenza HA head Ab (6649), reconstructed 564 unmutated common ancestor (564 UCA), and 564. Development for murine IgG (green), counterstained with DAPI (blue) and phalloidin (red). Overlay of all three channels (top row) or mIgG channel alone (bottom row).

(I) Representative examples of the different staining patterns observed for cloned sequences from single GC: perinuclear (G1_M25), predominantly cytoplasmic (G2_M05), cytoplasmic + nucleolar (G4_G22), and nuclear stain with nucleolar exclusion (G4_G55). Channel intensity was adjusted to facilitate visualization of the pattern.

(J) Quantified staining intensities based on CellProfiler analysis of raw images. Nuclear staining, cytoplasmic staining, and the sum of the two (left to right). Cloned antibodies are grouped according to GC origin as indicated. The threshold for background signal, defined as the upper limit of the 95% confidence interval for the mean signal in the negative control (6649), is indicated with a horizontal dotted line. Measurements for which the limit of the 95% confidence interval for the mean did not overlap with threshold were considered positive. Positive measurements are indicated in dark blue, while negative are light blue, and borderline are patterned. The positive control, hybridoma-derived 564 C11, is indicated in red.

See also Figure S3.

sequences (the CDR3 region being the most critical for Ag recognition) of clones carrying the VHQ52.a27.79 (IGHV2-9*02), J558.22.112 (IGHV1-22*01), and J558.33 (IGHV1S81*02) elements yielded hits for anti-DNA binding antibodies (including the original 564 VH clone) and anti-phosphocholine antibodies. These findings indicate that WT-derived GC B cells converged on specific autoreactive sequence elements.

To definitively determine whether BCRs from WT-derived clones were autoreactive, paired H and K chains from 16 clones and 1 inferred unmutated common ancestor (UCA) from 4 GCs of a PA-GFP 564Igi mixed chimera were synthesized, cloned, and expressed (Table S2). As controls, we cloned and expressed the original 564 Ab, the inferred 564 UCA, and an influenza hemagglutinin (HA)-specific Ab (6649). An overview of the sequence diversity of the 17 PA-GFP-derived clones and the 564 clone is shown in the phylogram in Figure 3G, which was rooted on the 564 UCA. The 20 total recombinant antibodies and the control 564 Ab derived from a hybridoma were assayed for cross-reactivity with cellular components in human epithelial (HEp-2) cells (Figures 3H–3J). Representative examples of the different staining patterns observed for cloned sequences from single GCs are shown in Figure 3I: perinuclear (G3_M25), predominantly cytoplasmic (G2_M05), cytoplasmic + nucleolar (G4_G22), and nuclear stain with nucleolar exclusion (G4_G55). Staining intensities were quantified in CellProfiler and are shown in Figure 3J.

Out of 4 GCs analyzed, autoreactivity was confirmed in 3. We further validated our findings in nucleolar ELISA-type assays (Figure S3F). The analysis was extended and refined by screening with autoAg arrays (Ayoglu et al., 2016), where each clone was assayed against 241 Ags (227 unique targets) and 30 controls (10 unique antibodies) (Table S3), and overall, results were congruent with the HEp-2 and nucleolar ELISA results (Figures S3G–S3K). The 564 clone, 564 UCA, G4_G22, and UCA GC2 were strongly reactive with single-stranded DNA (ssDNA) (Figure S3H). G2_M05 also reacted to ssDNA, but reacted most strongly with macrophage-derived chemokine (MDC, CCL22). Clones G2_G87, G2_G23, and G3_M25 displayed unique reactivity, albeit weaker, to this target (Figure S3I). These differences suggested a link between subcellular targeting and finer Ag specificity, because in the HEp-2-assay, G4_G22 and G2_M05 stained nucleolar + cytoplasmic and cytoplasmic, respectively, whereas G3_M25 had perinuclear staining. G4_G55, which had nuclear staining with nucleolar exclusion, was strongly reactive with Smith D2 Ag (Figure S3J). Interestingly, UCA_GC2 had additional reactivity to TGFβ-RII, not present in the other ssDNA-reactive clones (Figure S3K). The finding that the inferred UCA of the IgG-switched clones in GC2 was autoreactive suggests that germline precursors are autoreactive and enter GCs as such. Furthermore, there was CSR, as both autoreactive IgMs and IgGs were observed. Taken together, these results confirm that the spontaneous WT-derived GC B cells were autoreactive and were the likely source of the WT-derived, affinity-matured IgG2c autoantibodies observed in the chimeras.

GCs of 564Igi Mixed Chimeras Are T-Dependent with a Prominent Follicular Helper T Cell Population

GCs that form in response to foreign Ag depend on T cell help. To test whether those in 564Igi mice and 564Igi mixed chimeras do as well, we treated mice with anti-CD40L Ab to block T cell interaction. Similar to foreign Ag GCs, CD40L blockade ablated the GCs in spleen, cutaneous LN, and mesenteric LN of both heterozygous 564Igi mice and 564Igi mixed chimeras (Figures S4A–S4D). Splenic Id frequencies were unaffected, whereas those of cutaneous and mesenteric LN were marginally decreased. T follicular helper (Tfh, CXCR5^{hi}PD-1^{hi}) cell populations were present in both heterozygous 564Igi mice and 564Igi mixed chimeras, and they were similarly ablated by CD40L blockade, as previously shown (Durie et al., 1993; Yusuf et al., 2014). In contrast, overall CD4 T cell levels were unaffected (Figures S4E–S4H).

WT-Derived GC B Cells in 564Igi Mixed Chimeras Depend on TLR7 Signals

B cell-intrinsic TLR7 signaling is a driver of escape of tolerance for self-reactive B cells, as observed for Id^{+} cells in the 564Igi model (Berland et al., 2006; Green et al., 2012; Lau et al., 2005; Leadbetter et al., 2002). To test whether the WT-derived GC B cells in 564Igi mixed chimeras similarly depended on intrinsic TLR7 signaling, three-part mixed chimeras were generated using irradiated CD45.1/2 recipients. One part was 564Igi BM (identified by CD45.2 and PA-GFP congenic markers), one part was WT (CD45.1) BM, and the last part was either TLR7$^{-/-}$ or TLR7$^{+/+}$ BM (both CD45.2) (Figure 4A). Both TLR7$^{-/-}$ and TLR7$^{+/+}$ BM mixtures reconstituted mice equally, as demonstrated by near-expected (50:50) ratios of CD45.1 to CD45.2 T and B cells after excluding CD45.1/2 double-positive (recipient-derived) and PA-GFP-positive cells (564Igi-derived) (Figures S5A–S5H). Normal and comparable B and T cell frequencies were confirmed (Figures S5I–S5K). Robust and comparable GC frequencies were observed in both spleen and mesenteric LN for TLR7$^{-/-}$ and TLR7$^{+/+}$ chimeras, both in terms of total GC B cells and GC B cells after exclusion of PA-GFP and CD45.1/2 cells (Figures S5L and S5M).

There were significantly fewer TLR7$^{-/-}$ GC B cells than TLR7$^{+/+}$ GC B cells in the spleens of mixed chimeras (Figure 4B), meaning that WT B cells needed intrinsic TLR7 signaling for entry or persistence in autoreactive GCs. In mesenteric LN, there was a less dramatic, albeit significant, reduction in TLR7$^{-/-}$ cell frequency (Figure S5N). The reduced dependence on the TLR7 pathway in intestinal LN GCs is likely due to multiple other TLR ligands originating from gut flora or food Ags.

Spontaneous GCs of 564Igi Mixed Chimeras Become Self-Propagating

Because of the low frequency of 564-derived cells in the autoreactive GCs of mixed chimeras, we asked whether the GCs were dependent on 564Igi cells for their persistence or whether the epitope spreading was sufficient to maintain them. We crossed 564Igi mice with UBC-Cre^{ERT2} mice and a conditional attenuated-diphtheria toxin (DTA) line (564 UBC-Cre^{ERT2} DTA). The BM from these mice (CD45.2) were mixed with BM from PA-GFP WT mice (CD45.2) and transferred to irradiated WT recipients (CD45.1) (Figure 4C). This set-up allowed specific ablation of 564-derived cells in a tamoxifen-induced manner. Following reconstitution, a high degree of chimerism was verified, and the expected frequencies of donor and normal B cells were observed (Figures S5O–S5R).

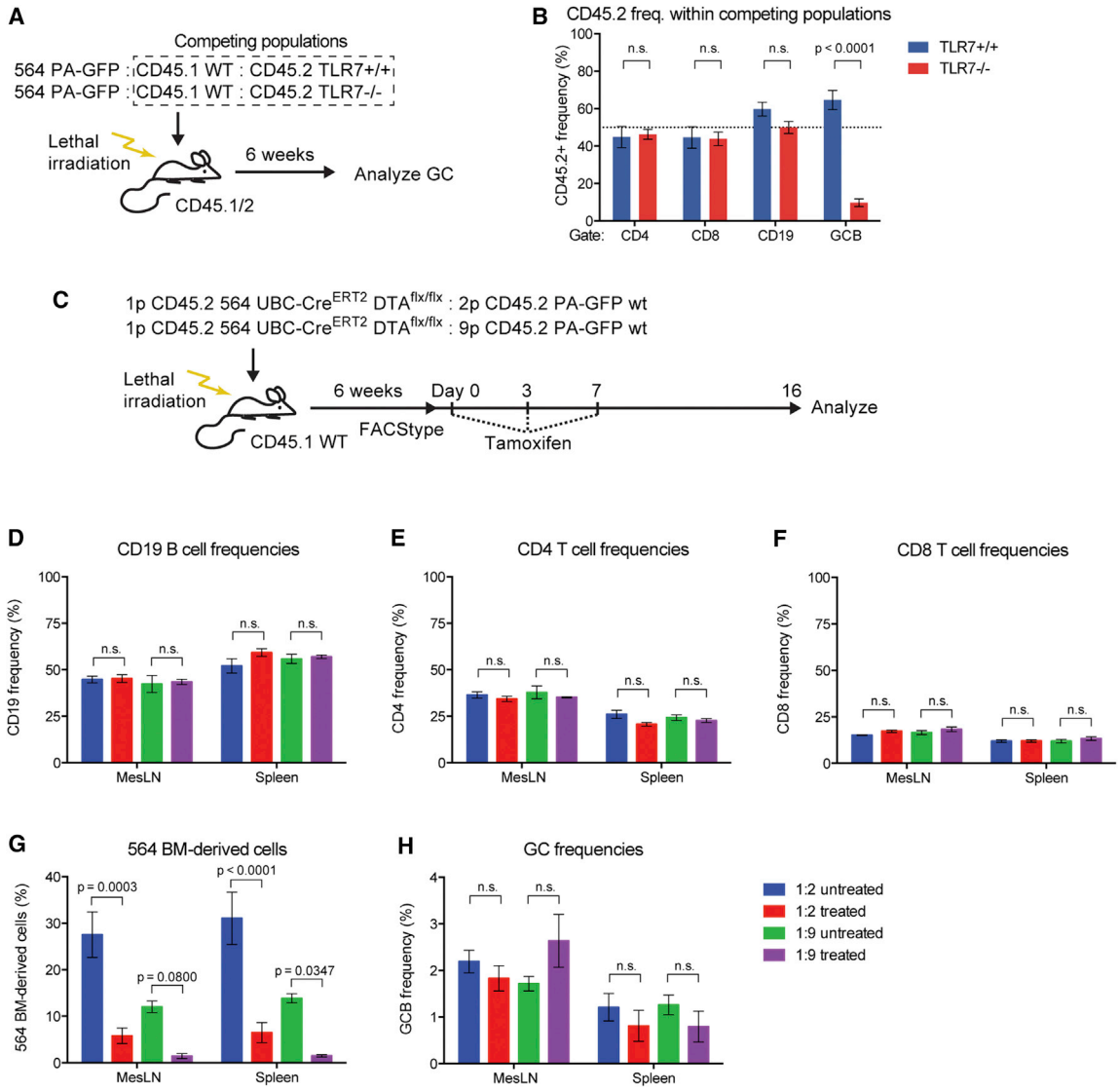

Figure 4. WT GCs Depend on B Cell-Intrinsic TLR7 Signaling and Become Self-Sustained

(A) Overview of experimental approach for generation and analysis of $TLR7^{+/+}$ and $TLR7^{-/-}$ mixed 564 chimeras.

(B) Splenic CD45.2 frequencies in the competition gate within CD4, CD8, CD19, and GC B populations of $TLR7^{+/+}$ (n = 3) and $TLR7^{-/-}$ (n = 4) mixed 564 chimeras. Mean ± SEM, multiplicity-adjusted p values for two-way ANOVA with Dunnett's posttest. Dotted line indicates the expected 50% frequency.

(C) Overview of experimental layout for generating and analyzing 564 DTA mixed chimeras.

(D) CD19 frequencies of untreated versus treated 1:2 and 1:9 564 DTA mixed chimeras. Mean ± SEM for 3 mice per group, multiplicity-adjusted p values for 2-way ANOVA with Tukey's posttest, n.s., not significant.

(E) Similar to (D) but showing CD4 frequencies.

(F) Similar to (D) but showing CD8 frequencies.

(G) Similar to (D) but showing 564 BM-derived cell frequencies.

(H) Similar to (D) but showing GC B cell frequencies.

See also Figures S4 and S5.

Half the cohort was treated with tamoxifen and mice were analyzed 2 weeks later. As expected, overall CD4 T cell, CD8 T cell, and CD19 B cell frequencies were unaffected (Figures 4D–4F). Because the frequency of 564-derived B cells was already low and therefore harder to quantify, CD8 T cells were used to measure the ablation strategy's effect on the 564-derived hematopoietic compartment. In the 1:2 chimeras, the 564-derived cell frequency was reduced ~80% (from ~30% down to ~6%); whereas in the 1:9 chimeras, it was reduced ~90% (from ~12% down to ~1.2%) (Figure 4G). Despite this dramatic reduction in 564-derived cells, splenic and mesenteric GC B cell frequencies were only marginally reduced (Figure 4H). Therefore, 564-derived cells were not required once autoreactive GCs had been established.

Autoreactive GCs Evolve toward Pauciclonality

To analyze autoreactive GC dynamics globally, we generated mixed 564Igi and Aid-Cre^{ERT2} Confetti BM chimeras. In this setup, 564-driver cells elicit autoreactive GCs largely composed of WT-derived Aid-Cre^{ERT2} Confetti B cells. Upon tamoxifen induction, Aid^{+} (GC) cells and their progeny express 1 of 10 different color combinations, allowing the visualization of clonal selection, as previously done for foreign Ag (Tas et al., 2016).

Robust induction of autoreactive GCs was observed, and the autoreactive GCs were composed of WT clones as evidenced by Confetti positivity (Movies S3 and S4). As an internal control, "Confetti only" chimeras without 564 driver BM were generated and immunized with a foreign Ag (NP-CGG) analogous to that of Tas et al. (2016) (Figure 5A). Over 4 weeks, foreign-Ag-elicited GCs lost color diversity, as evidenced by the frequencies of the most dominant and second-most dominant color and the sum of the two relative to the remainder of the GC (Figures 5B and 5E). Unlike for Tas et al. (2016), these data do not account for unrecombined cells, and therefore, the results are not directly comparable.

However, we found that the autoreactive GCs evolved in a similar manner as foreign-Ag GCs, losing color diversity at only a slightly decreased rate (Figures 5C and 5E), which was confirmed by comparing the divergence index for the two groups (Figure 5D). Of note, whereas foreign-Ag-induced GCs are synchronized and timed, the 564Igi GCs were spontaneous and chronic, making it difficult to determine GC age. However, the effect of GC age could be controlled for by comparing to mesenteric LN GCs, which are chronic, in both groups. Notably, we observed no difference between the mesenteric LN GCs of foreign-Ag-immunized Confetti-only mice and those of 564Igi chimeric mice (Figures S6A–S6I), indicating that there is no effect from GC age. We conclude that autoreactive GCs, once tolerance has been broken, evolve toward pauciclonality—that is, the dominance of a single or a few clones and their progeny.

Mixed 564Igi Chimeras Undergo Epitope Spreading

Given the differential Vh usage and clonal selection of WT-derived GC B cells, we hypothesized that the WT-derived response may target more self-Ags than the original 564Igi clone. IgG (total), IgG2a (564-derived), and IgG2c (WT-derived) from 9 heterozygous 564Igi, 7 homozygous 564Igi, 6 1:2 564 mixed chimeras, 2 1:9 564 mixed chimeras, 6 1:2 564K^{-} mixed chimeras, and 5 B6 mice were assayed for binding to 241 Ags (227 unique targets) and 30 controls (10 unique Abs) (Figures S7A–S7C; Table S3). Individual mice within each group varied in reactivity, but the IgG antibodies of heterozygous 564Igi mice, homozygous 564Igi mice, and 564Igi mixed chimeras had stronger reactivity across a broad range of self-Ags than did IgG from 564K^{-} mixed chimeras and B6 mice (Figure S7A). IgG2a (564-derived) was strongly reactive in homozygous 564Igi and to a lesser extent heterozygous 564Igi mice (Figure S7B), whereas IgG2c (WT-derived) was strongly reactive in 564Igi mixed chimeras (Figure S7C), agreeing with the preceding experiments. A shift, or broadening, of reactivities was notable when comparing 564Igi mixed chimeras and homozygous 564Igi mice, which have B cells that are doubly pre-arranged and so cannot easily acquire new targets (Figure 6A). TNF-β (tumor necrosis factor beta), GBM (glomerular basement membrane), and numerous other targets were significantly overrepresented in the mixed chimeras (upper right quadrant, Figure 6A). Many of these targets are well-established autoimmune targets (GBM, collagen type VI, U1-snRNP A, etc.) including cytokines (APRIL, VEGF, interleukin [IL]-17, etc.) (Cappellano et al., 2012).

The original 564 clone did not react with interferon (IFN)γ, GBM, SmD2 (Smith D2), or TNF-β, suggesting that these are targets of WT-derived autoreactive B cells (IgG and IgG2c) (Figures 6B, 6C, S7D, and S7E). The 564 clone reacts with ssDNA (Berland et al., 2006; Gavalchin et al., 1987) (compare also with Figure S3), so not surprisingly, ssDNA and Ro60/SSA were the most notable 564-associated targets (upper left quadrant, Figure 6A). Homozygous 564Igi and to a lesser extent heterozygous 564Igi mice had a strong anti-ssDNA profile for IgG and IgG2a (564-derived), but not for IgG2c (WT-derived) (Figure S7D). 564Igi mixed chimeras had a significant but lower level of anti-ssDNA IgG and IgG2a than homozygous and heterozygous 564Igi mice, whereas 564K^{-} mixed chimeras had none (Figure S7E). A similar pattern was noted for Ro60/SSA (Figures 6B and C), in line with the polyreactive nature of the parental 564 clone. Taken together, these results suggest that inclusion of WT B cells in chronic autoreactive GCs drives epitope spreading.

Mixed 564Igi Chimeras Have Ab Deposits in Their Kidneys

The reactivity of 564Igi mixed chimeras toward GBM and collagen type IV suggested autoAb deposition in their kidneys, as those antigens are often targeted in autoimmune renal disease. We found that aged (9–12 months old) heterozygous 564Igi mice and 564Igi mixed chimeras had prominent IgG2c (WT-derived) deposits in the kidney; whereas, homozygous 564Igi and homozygous 564Igi K^{-} mice did not (Figures 7A and 7B). As expected, IgG2a (knockin allele) deposits were prominent in homozygous 564Igi mice, as well as 564Igi mixed chimeras, but were not detected in the homozygous 564Igi K^{-} mice (Figures 7A and 7C). This IgG2c deposition suggests a contribution of the epitope spreading process to pathogenesis.

DISCUSSION

We made the unexpected observation of widespread epitope spreading in the 564Igi model. In heterozygous 564Igi mice, upward of half of circulating naive mature B cells carried an affinity-matured autoreactive BCR derived from the knockin. Yet, these cells failed to win in the GC reaction, giving way to WT-derived cells. This was surprising, because in mice that have a knockin BCR that is specific for foreign Ag, the knockin B cells dominate the GC response. For example, in B1-8 mice, 5% of the pool harbor a BCR specific for the hapten NP, and upon NP-carrier immunization, these cells dominate the response. However, this is arguably an oversimplified system as the hapten response is very narrow. Our findings in the autoreactive setting may reflect those of Kuraoka et al. (2016), whereby the process of SHM increases the breadth of the response to complex Ag.

Although the maturation of autoreactive BCRs is generally restricted by T cell support, this check may be bypassed by linked recognition. In fact, autoreactive IgG memory antibodies

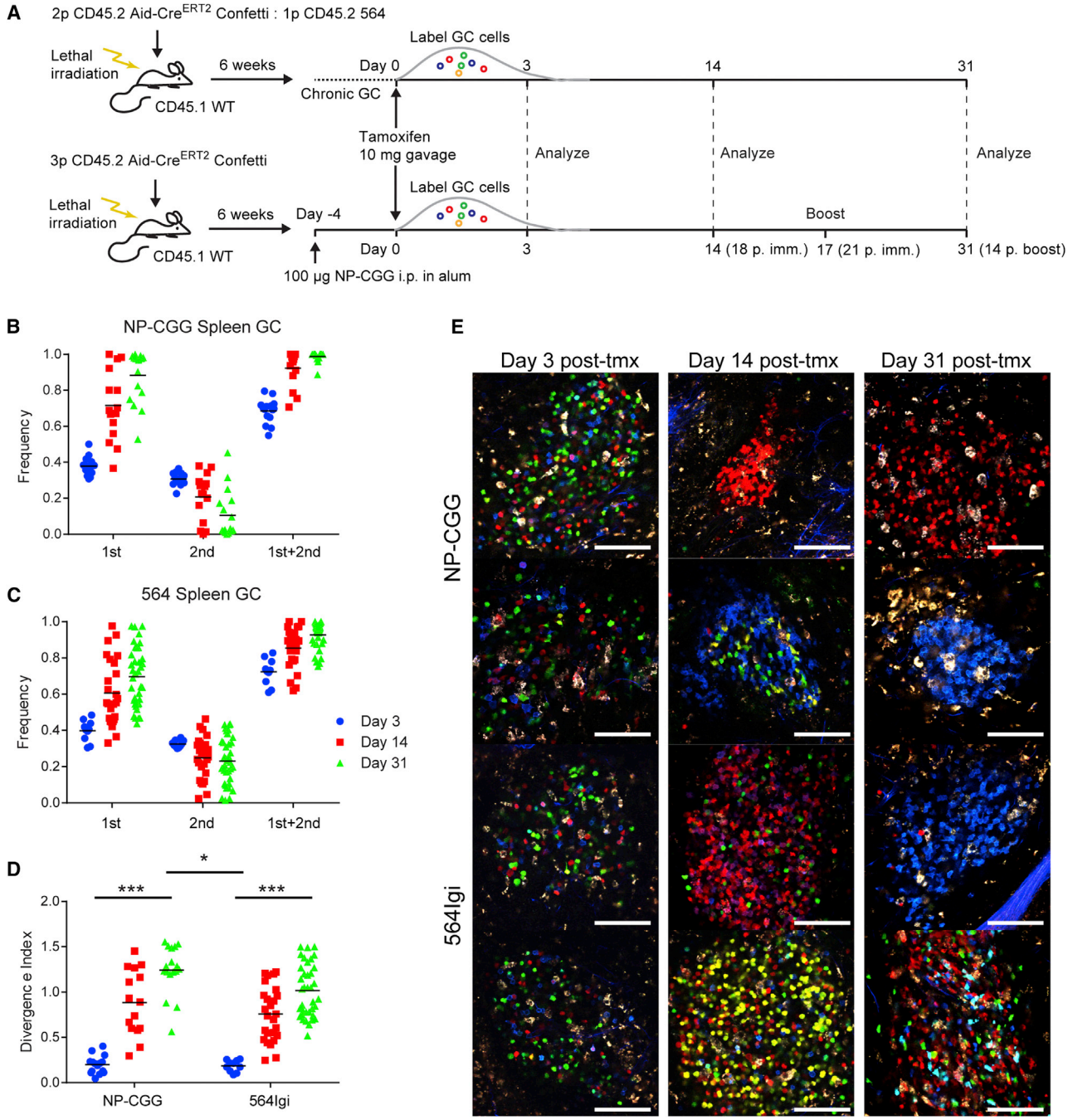

Figure 5. Clonal Evolution in Autoreactive GCs in the Aid-Confetti Model

(A) Overview of experimental setup for generating and analyzing Aid-Cre^{ERT2} Confetti mixed 564 chimeras.

(B) Frequency of most frequent color (1st), second-most frequent color (2nd) and their sum observed in individual splenic GC at Day 3, 14, and 31 post-tamoxifen induction of Confetti recombination in NP-CGG-immunized Confetti chimeras. The mean of an average of 7.8 GC per spleen for 2 mice per time point is indicated by the bar.

(C) As (B), but for 564 Confetti mixed chimeras. The mean of an average of 9.2 GC per spleen for 3 mice per time point is indicated by the bar.

(D) Divergence index for the GC represented in (B) and (C). Significance indicated for two-way ANOVA with Tukey's posttest (*$p < 0.05$, ***$p < 0.001$).

(E) Representative images used for quantification of color dominance. The scale bars indicate 100 µm.

See also Figure S6 and Movies S3 and S4.

in patients with SLE may arise from nonreactive and polyreactive precursors (Mietzner et al., 2008). However, mechanisms may exist to prevent the emergence of autoreactive B cells in GCs (Reed et al., 2016; Sabouri et al., 2014), perhaps relying in part on FDC presentation of autoAg (Yau et al., 2013). The nature of the self-Ag may be an important factor, as many nuclear

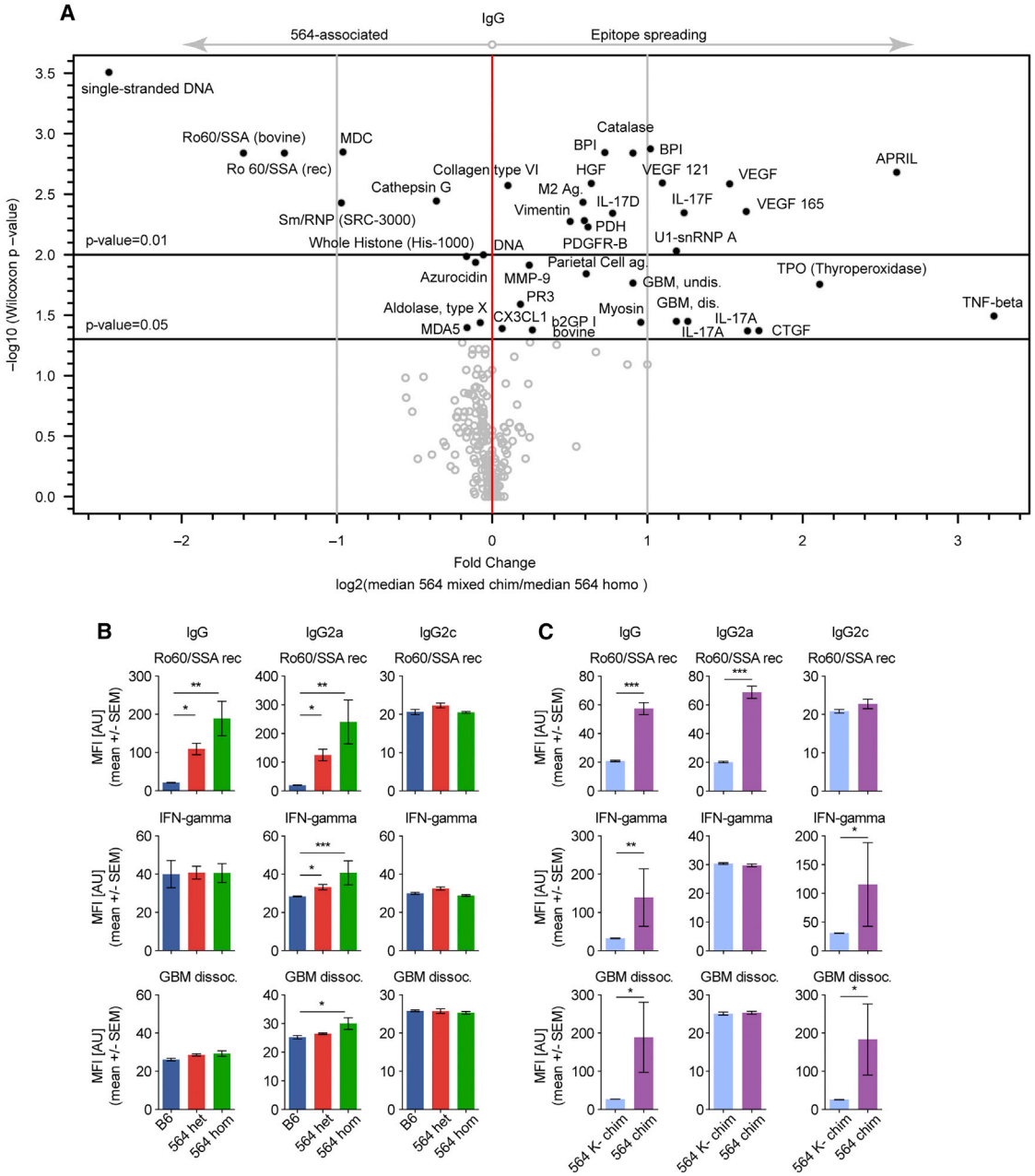

Figure 6. The Convergence on Stereotypic Autoreactive Sequence Elements Is Mirrored Serologically by Functional Epitope Spreading

(A) Volcano plot comparison of median IgG signal intensities in 564 mixed chimeras (n = 8) relative to homozygous 564Igi mice (n = 7), with indication of log2-fold change on the x axis and significance level on the y axis.

(B) Bar graph representations of IgG (left column), IgG2a (middle column) and IgG2c (right column) Ab toward Ro60/SSA (top row), IFNγ (middle row), and dissociated GBM (bottom row) in sera of B6 (n = 5), heterozygous (n = 9), and homozygous (n = 7) 564Igi mice. Mean ± SEM, multiplicity-adjusted significance for one-way ANOVA with Dunn's posttest (*p < 0.05, **p < 0.01, ***p < 0.001).

(C) Bar graph representations of IgG (left column), IgG2a (middle column), and IgG2c (right column) Ab toward Ro60/SSA (top row), IFNγ (middle row), and dissociated GBM (bottom row) in sera of 564 mixed chimeras (n = 8) and 564K^{-} mixed chimeras (n = 6). Mean ± SEM, multiplicity-adjusted significance for two-tailed Mann-Whitney test (*p < 0.05, **p < 0.01, ***p < 0.001).

See also Figure S7.

self-Ags, such as the 564Igi Ag, trigger FDCs to secrete IFNα via endosomal TLR7 (Das et al., 2017), potentially leading to increased recruitment of self-reactive B cells from the immature repertoire.

To circumvent artifacts that might arise from transgenic B cells, we developed a mixed chimera model with spontaneous, autoreactive GCs composed of WT B cells with 564Igi cells

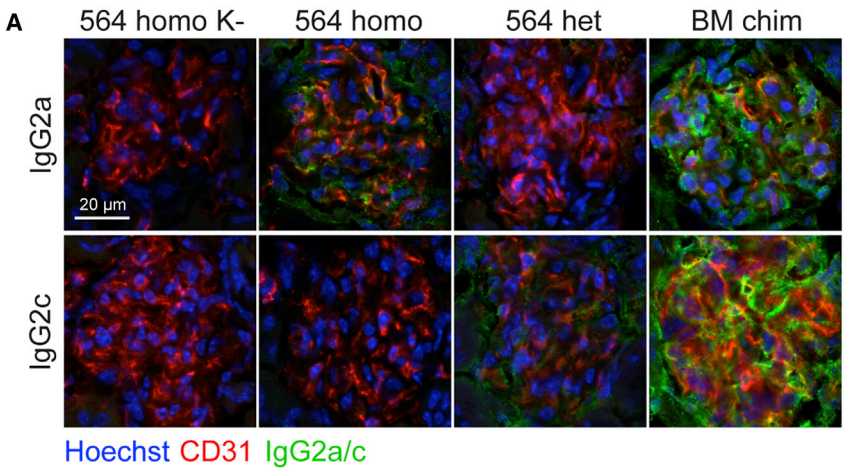

Figure 7. WT-Derived Autoantibodies Are Deposited in Kidneys of 564Igi Mice and 564Igi Mixed Chimeras

(A) Representative immunofluorescence analysis of IgG2a (top) and IgG2c (bottom) deposition in glomeruli of kidneys from a homozygous 564Igi K^{-} control, a homozygous 564Igi, a homozygous 564Igi mouse, and a 564Igi mixed chimera. Glomerular vessels defined by CD31 (red), nuclei counterstained with Hoechst (blue), Ab deposits in green.

(B) Quantification of IgG2c Ab deposits within the glomerular area defined by CD31 staining. The analysis was based on an average of 2.5 images from each mouse for 564 homo K^{-} (n = 1), 564 homo (n = 1), 564het (n = 2), and 564 mixed chimeras (n = 3). Statistical significance for Kruskal-Wallis test with Dunn's posttest (**$p < 0.01$).

(C) Similar to (B) but for IgG2a.

initiating autoimmunity. We found that these autoreactive GCs are largely composed of WT B cells and are dependent on intrinsic TLR7 signaling, similarly to 564Igi B cells (Berland et al., 2006). Moreover, we found that the GCs became self-sustained and gained independence from the initial 564Igi trigger, explaining how autoreactive GCs become chronic and how disease is propagated.

We found that autoreactive GCs are polyclonal, but evolve toward pauciclonality at varying rates, agreeing with the observation that affinity maturation can occur in the absence of homogenizing selection, with many clones maturing in parallel within the same GC (Tas et al., 2016). This "clonal permissiveness" is in line with earlier reports that transient foreign-Ag-driven GCs are dynamic and open structures (Schwickert et al., 2007, 2009). We found that clonal evolution was largely similar between foreign Ag and autoAg GCs. Our observations suggest that once tolerance is broken, an increasingly broader array of self-Ags will be targeted.

We observed clonal convergence and selection leading to the predominance of autoreactive V segments in the WT-derived GC B cell population, similar to previous observations in autoimmunity and cancer (Hershberg and Luning Prak, 2015; Shlomchik et al., 1987). Serum antibodies displayed epitope spreading, further supported by our finding of WT-derived Ab deposits (IgG2c) in the kidneys of 564Igi mixed chimeras.

Our findings support that autoreactive GCs are at the heart of the autoimmune response. The chronic, progressive nature of epitope spreading calls for early interventions, even before disease onset. In light of the failure of CD40L blockade in humans, alternative GC checkpoints should be explored. We have focused here on the evolution of the B cell response, but questions remain. Although we demonstrated T cell dependence in our model, the extent and nature of T cell involvement has not been addressed. Future experiments will determine whether the T cell pool is not only necessary, but also sufficient, to sustain and confer autoreactivity.

We conclude that self-reactive 564Igi B cells are sufficient to break tolerance and induce the formation of autoreactive GCs, which are predominantly composed of WT-derived cells. We dub this novel tool, which can be used to study WT epitope spreading and autoreactive GC responses, the "ARTEMIS model" to signify autoreactive B cell driven T-dependent epitope migration toward immunity to self.

STAR★METHODS

Detailed methods are provided in the online version of this paper and include the following:

- KEY RESOURCES TABLE
- CONTACT FOR REAGENT AND RESOURCE SHARING
- EXPERIMENTAL MODEL AND SUBJECT DETAILS
  - Mice
  - Cells
- METHOD DETAILS
  - Antibodies and staining reagents
  - Genotyping and FACStyping
  - Chimeras
  - Additional procedures
  - Mutiphoton imaging and photoactivation of explants
  - Confetti analyses
  - Flow cytometry
  - Bulk sequence analysis
  - Single cell sequence analysis

- Clonal lineage determination and inference
- Cloning, expression and purification of IgGs
- Nucleolar ELISA/TRIFMA
- Immunofluorescence confocal microscopy
- HEp-2 Immunofluorescence assay
- Image analysis
- Autoantigen arrays

- QUANTIFICATION AND STATISTICAL ANALYSIS
- DATA AND SOFTWARE AVAILABILITY

SUPPLEMENTAL INFORMATION

Supplemental Information includes seven figures, three tables, and four movies and can be found with this article online at http://dx.doi.org/10.1016/j.cell.2017.07.026.

AUTHOR CONTRIBUTIONS

S.E.D. conceived the project. S.E.D., C.E.v.d.P., D.J.F., B.A., F.A.A.Q., and G.B. planned and performed experiments and analyzed data. C.E.v.d.P. and D.J.F. contributed equally. L.M., C.-A.R., J.-C.W., P.J.U., and G.D.V. provided crucial reagents and expertise. P.J.U., G.D.V., and M.C.C. oversaw the project. S.E.D. wrote the manuscript. All authors provided critical feedback.

ACKNOWLEDGMENTS

We thank H. Leung of the Optical Microscopy Core and N. Barteneva and K. Ketman of the Flow and Imaging Cytometry Resource at the PCMM for technical assistance. We also thank the SciLifeLab Autoimmunity Profiling Facility for access to FlexMap3D instrument. We are grateful to E. Alicot for technical assistance, D. Weseman for helpful discussion of the topic, and C. Usher for help editing the manuscript. F. Alt provided the attenuated DTA strain and A. Sharpe the UBC-Cre^{ERT2} line. S.E.D. was supported by the Benzon Foundation and by a Marie Curie International Outgoing Fellowship within the 7th European Community Framework Programme (PIOF-GA-2012-330134). C.E.v.d.P. was supported by a fellowship from GSK. D.J.F. was supported by the HHMI Medical Research Fellows Program. B.A. was supported by the Knut and Alice Wallenberg Foundation Postdoctoral Scholarship Program (KAW 2014.0412). This research was supported by NIH grants R01AI039246, R21AI117737 (M.C.C.), R01AI119006 (G.D.V.), U19AI110491, UM1AI110498, and R01 AI125197 (P.J.U.), by the Donald E. and Delia B. Baxter Foundation (Career Development Award to P.J.U.), the Henry Gustav Floren Trust (gift to P.J.U.), and a gift from Elizabeth F. Adler (to P.J.U.).

Received: December 6, 2016
Revised: May 17, 2017
Accepted: July 14, 2017
Published: August 24, 2017

REFERENCES

Arbuckle, M.R., McClain, M.T., Rubertone, M.V., Scofield, R.H., Dennis, G.J., James, J.A., and Harley, J.B. (2003). Development of autoantibodies before the clinical onset of systemic lupus erythematosus. N. Engl. J. Med. *349*, 1526–1533.

Ayoglu, B., Mitsios, N., Kockum, I., Khademi, M., Zandian, A., Sjöberg, R., Forsström, B., Bredenberg, J., Lima Bomfim, I., Holmgren, E., et al. (2016). Anoctamin 2 identified as an autoimmune target in multiple sclerosis. Proc. Natl. Acad. Sci. USA *113*, 2188–2193.

Berland, R., Fernandez, L., Kari, E., Han, J.-H., Lomakin, I., Akira, S., Wortis, H.H., Kearney, J.F., Ucci, A.A., and Imanishi-Kari, T. (2006). Toll-like receptor 7-dependent loss of B cell tolerance in pathogenic autoantibody knockin mice. Immunity *25*, 429–440.

Busse, C.E., Czogiel, I., Braun, P., Arndt, P.F., and Wardemann, H. (2014). Single-cell based high-throughput sequencing of full-length immunoglobulin heavy and light chain genes. Eur. J. Immunol. *44*, 597–603.

Cappellano, G., Orilieri, E., Woldetsadik, A.D., Boggio, E., Soluri, M.F., Comi, C., Sblattero, D., Chiocchetti, A., and Dianzani, U. (2012). Anti-cytokine autoantibodies in autoimmune diseases. Am. J. Clin. Exp. Immunol. *1*, 136–146.

Chatterjee, P., Agyemang, A.F., Alimzhanov, M.B., Degn, S., Tsiftsoglou, S.A., Alicot, E., Jones, S.A., Ma, M., and Carroll, M.C. (2013). Complement C4 maintains peripheral B-cell tolerance in a myeloid cell dependent manner. Eur. J. Immunol. *43*, 2441–2450.

Cornaby, C., Gibbons, L., Mayhew, V., Sloan, C.S., Welling, A., and Poole, B.D. (2015). B cell epitope spreading: mechanisms and contribution to autoimmune diseases. Immunol. Lett. *163*, 56–68.

Das, A., Heesters, B.A., Bialas, A., O'Flynn, J., Rifkin, I.R., Ochando, J., Mittereder, N., Carlesso, G., Herbst, R., and Carroll, M.C. (2017). Follicular dendritic cell activation by TLR ligands promotes autoreactive B cell responses. Immunity *46*, 106–119.

Dogan, I., Bertocci, B., Vilmont, V., Delbos, F., Mégret, J., Storck, S., Reynaud, C.-A., and Weill, J.-C. (2009). Multiple layers of B cell memory with different effector functions. Nat. Immunol. *10*, 1292–1299.

Durie, F.H., Fava, R.A., Foy, T.M., Aruffo, A., Ledbetter, J.A., and Noelle, R.J. (1993). Prevention of collagen-induced arthritis with an antibody to gp39, the ligand for CD40. Science *261*, 1328–1330.

Gavalchin, J., Seder, R.A., and Datta, S.K. (1987). The NZB X SWR model of lupus nephritis. I. Cross-reactive idiotypes of monoclonal anti-DNA antibodies in relation to antigenic specificity, charge, and allotype. Identification of interconnected idiotype families inherited from the normal SWR and the autoimmune NZB parents. J. Immunol. *138*, 128–137.

Green, N.M., Moody, K.-S., Debatis, M., and Marshak-Rothstein, A. (2012). Activation of autoreactive B cells by endogenous TLR7 and TLR3 RNA ligands. J. Biol. Chem. *287*, 39789–39799.

Han, S., Zheng, B., Dal Porto, J., and Kelsoe, G. (1995). In situ studies of the primary immune response to (4-hydroxy-3-nitrophenyl)acetyl. IV. Affinity-dependent, antigen-driven B cell apoptosis in germinal centers as a mechanism for maintaining self-tolerance. J. Exp. Med. *182*, 1635–1644.

Herlands, R.A., Christensen, S.R., Sweet, R.A., Hershberg, U., and Shlomchik, M.J. (2008). T cell-independent and toll-like receptor-dependent antigen-driven activation of autoreactive B cells. Immunity *29*, 249–260.

Hershberg, U., and Luning Prak, E.T. (2015). The analysis of clonal expansions in normal and autoimmune B cell repertoires. Philos. Trans. R. Soc. Lond. B Biol. Sci. *370* http://dx.doi.org/10.1098/rstb.2014.0239.

Kepler, T.B. (2013). Reconstructing a B-cell clonal lineage. I. Statistical inference of unobserved ancestors. F1000Res. *2*, 103.

Kuraoka, M., Schmidt, A.G., Nojima, T., Feng, F., Watanabe, A., Kitamura, D., Harrison, S.C., Kepler, T.B., and Kelsoe, G. (2016). Complex antigens drive permissive clonal selection in germinal centers. Immunity *44*, 542–552.

Lamprecht, M.R., Sabatini, D.M., and Carpenter, A.E. (2007). CellProfiler: free, versatile software for automated biological image analysis. Biotechniques *42*, 71–75.

Lau, C.M., Broughton, C., Tabor, A.S., Akira, S., Flavell, R.A., Mamula, M.J., Christensen, S.R., Shlomchik, M.J., Viglianti, G.A., Rifkin, I.R., and Marshak-Rothstein, A. (2005). RNA-associated autoantigens activate B cells by combined B cell antigen receptor/Toll-like receptor 7 engagement. J. Exp. Med. *202*, 1171–1177.

Leadbetter, E.A., Rifkin, I.R., Hohlbaum, A.M., Beaudette, B.C., Shlomchik, M.J., and Marshak-Rothstein, A. (2002). Chromatin-IgG complexes activate B cells by dual engagement of IgM and Toll-like receptors. Nature *416*, 603–607.

Luning Prak, E.T., Monestier, M., and Eisenberg, R.A. (2011). B cell receptor editing in tolerance and autoimmunity. Ann. N Y Acad. Sci. *1217*, 96–121.

Luzina, I.G., Atamas, S.P., Storrer, C.E., daSilva, L.C., Kelsoe, G., Papadimitriou, J.C., and Handwerger, B.S. (2001). Spontaneous formation of germinal centers in autoimmune mice. J. Leukoc. Biol. *70*, 578–584.

Mietzner, B., Tsuiji, M., Scheid, J., Velinzon, K., Tiller, T., Abraham, K., Gonzalez, J.B., Pascual, V., Stichweh, D., Wardemann, H., and Nussenzweig, M.C. (2008). Autoreactive IgG memory antibodies in patients with systemic lupus erythematosus arise from nonreactive and polyreactive precursors. Proc. Natl. Acad. Sci. USA *105*, 9727–9732.

Pulendran, B., Kannourakis, G., Nouri, S., Smith, K.G.C., and Nossal, G.J.V. (1995). Soluble antigen can cause enhanced apoptosis of germinal-centre B cells. Nature *375*, 331–334.

R Development Core Team (2008). R: A language and environment for statistical computing (R Foundation for Statistical Computing).

Rahman, A., and Isenberg, D.A. (2008). Systemic lupus erythematosus. N. Engl. J. Med. *358*, 929–939.

Reed, J.H., Jackson, J., Christ, D., and Goodnow, C.C. (2016). Clonal redemption of autoantibodies by somatic hypermutation away from self-reactivity during human immunization. J. Exp. Med. *213*, 1255–1265.

Sabouri, Z., Schofield, P., Horikawa, K., Spierings, E., Kipling, D., Randall, K.L., Langley, D., Roome, B., Vazquez-Lombardi, R., Rouet, R., et al. (2014). Redemption of autoantibodies on anergic B cells by variable-region glycosylation and mutation away from self-reactivity. Proc. Natl. Acad. Sci. USA *111*, E2567–E2575.

Schwickert, T.A., Lindquist, R.L., Shakhar, G., Livshits, G., Skokos, D., Kosco-Vilbois, M.H., Dustin, M.L., and Nussenzweig, M.C. (2007). In vivo imaging of germinal centres reveals a dynamic open structure. Nature *446*, 83–87.

Schwickert, T.A., Alabyev, B., Manser, T., and Nussenzweig, M.C. (2009). Germinal center reutilization by newly activated B cells. J. Exp. Med. *206*, 2907–2914.

Shlomchik, M.J., Marshak-Rothstein, A., Wolfowicz, C.B., Rothstein, T.L., and Weigert, M.G. (1987). The role of clonal selection and somatic mutation in autoimmunity. Nature *328*, 805–811.

Shokat, K.M., and Goodnow, C.C. (1995). Antigen-induced B-cell death and elimination during germinal-centre immune responses. Nature *375*, 334–338.

Tas, J.M.J., Mesin, L., Pasqual, G., Targ, S., Jacobsen, J.T., Mano, Y.M., Chen, C.S., Weill, J.-C., Reynaud, C.-A., Browne, E.P., et al. (2016). Visualizing antibody affinity maturation in germinal centers. Science *351*, 1048–1054.

Tiller, T., Tsuiji, M., Yurasov, S., Velinzon, K., Nussenzweig, M.C., and Wardemann, H. (2007). Autoreactivity in human IgG+ memory B cells. Immunity *26*, 205–213.

Tiller, T., Busse, C.E., and Wardemann, H. (2009). Cloning and expression of murine Ig genes from single B cells. J. Immunol. Methods *350*, 183–193.

Vanderlugt, C.L., and Miller, S.D. (2002). Epitope spreading in immune-mediated diseases: implications for immunotherapy. Nat. Rev. Immunol. *2*, 85–95.

Victora, G.D., Schwickert, T.A., Fooksman, D.R., Kamphorst, A.O., Meyer-Hermann, M., Dustin, M.L., and Nussenzweig, M.C. (2010). Germinal center dynamics revealed by multiphoton microscopy with a photoactivatable fluorescent reporter. Cell *143*, 592–605.

Vinuesa, C.G., Sanz, I., and Cook, M.C. (2009). Dysregulation of germinal centres in autoimmune disease. Nat. Rev. Immunol. *9*, 845–857.

William, J., Euler, C., Christensen, S., and Shlomchik, M.J. (2002). Evolution of autoantibody responses via somatic hypermutation outside of germinal centers. Science *297*, 2066–2070.

Yau, I.W., Cato, M.H., Jellusova, J., Hurtado de Mendoza, T., Brink, R., and Rickert, R.C. (2013). Censoring of self-reactive B cells by follicular dendritic cell-displayed self-antigen. J. Immunol. *191*, 1082–1090.

Ye, J., Ma, N., Madden, T.L., and Ostell, J.M. (2013). IgBLAST: an immunoglobulin variable domain sequence analysis tool. Nucleic Acids Res. *41*, W34–W40.

Yusuf, I., Stern, J., McCaughtry, T.M., Gallagher, S., Sun, H., Gao, C., Tedder, T., Carlesso, G., Carter, L., Herbst, R., and Wang, Y. (2014). Germinal center B cell depletion diminishes CD4+ follicular T helper cells in autoimmune mice. PLoS ONE *9*, e102791.

STAR★METHODS

KEY RESOURCES TABLE

REAGENT or RESOURCE	SOURCE	IDENTIFIER
Antibodies		
Rabbit polyclonal anti-B-Phycoerythrin	Rockland Immunochemicals	Cat#200-401-099; RRID: AB_10893993
Rabbit polyclonal anti-C3b-A633	This paper	N/A
Rat monoclonal anti-mouse/human GL7 antigen-PacBlue (clone GL7)	Biolegend	Cat#144613; RRID: AB_2563291
Rat monoclonal anti-mouse/human CD45R/B220-PerCP/Cy5.5 (clone RA3-6B2)	Biolegend	Cat#103235; RRID: AB_893356
Mouse monoclonal anti-mouse IgM^b-FITC (clone AF6-78)	Biolegend	Cat#406205; RRID: AB_315038
Mouse monoclonal anti-mouse IgM^a-PE (clone MA-69)	Biolegend	Cat#408608; RRID: AB_940545
Mouse monoclonal anti-mouse CD45.1-FITC (clone A20)	Biolegend	Cat#110705; RRID: AB_313494
Mouse monoclonal anti-mouse CD45.2-APC (clone 104)	Biolegend	Cat#109813; RRID: AB_389210
Rat monoclonal anti-mouse IgD-PacBlue (clone 11-26c.2a)	Biolegend	Cat#405711; RRID: AB_1937245
Rat monoclonal anti-mouse CD21/CD35 (CR2/CR1)-PE (clone 7E9)	Biolegend	Cat#123409; RRID: AB_940411
Rat monoclonal anti-mouse CD138 (Syndecan-1)-PE (clone 281-2)	Biolegend	Cat#142503; RRID: AB_10915989
Rat monoclonal anti-mouse CD38-PE/Cy7 (clone 90)	Biolegend	Cat#102717; RRID: AB_2072892
Rat anti-mouse CD31-A647 (clone 390)	Biolegend	Cat#102415 RRID: AB_493411
Mouse monoclonal anti-mouse CD157 (BST-1)-PE (clone BP-3)	Biolegend	Cat#140203; RRID: AB_10643273
Mouse monoclonal anti-mouse CD95 (APO-1/Fas)-PE (clone 15A7)	eBioscience	Cat#12-0951-81; RRID: AB_465788
Rabbit polyclonal anti-Goat IgG (H+L) Cross-adsorbed-A488	ThermoFisher Scientific	Cat#A-11078; RRID: AB_2534122
Goat polyclonal anti-Mouse IgG_{2c}, Human adsorbed-AP	Southern Biotech	Cat#1079-04
Goat polyclonal anti-Mouse IgG_{2a}, Human adsorbed-AP	Southern Biotech	Cat#1080-04
Rabbit polyconal anti-Mouse Immunoglobulins-biotin	DAKO	Cat#E035401-2
Mouse monoclonal anti-idiotype (clone 9D11)	(Chatterjee et al., 2013)	N/A
Chemicals, Peptides, and Recombinant Proteins		
Tamoxifen	Sigma	Cat#T5648
Imject Alum Adjuvant	ThermoFisher Scientific	Cat#77161
Np-Osu	Bioresearch technologies	Cat#N-1010-100
Chicken gamma globulin	Rockland Immunochemicals	Cat#D602-0100
B-Phycoerythrin	ThermoFisher Scientific	Cat#P800
Fixable Viability Dye eFluor 780	eBioscience	Cat#65-0865-14
Hoechst 33342	ThermoFisher Scientific	Cat#H3570
Streptavidin-PE/Cy7	Biolegend	Cat#405206
Phalloidin-A568	ThermoFisher Scientific	Cat#A12380
DAPI (4',6-Diamidino-2-Phenylindole, Dihydrochloride)	ThermoFisher Scientific	Cat#D1306
Europium-labeled streptavidin	Perkin Elmer	Cat#1244-360
Deposited Data		
Heavy chain Ig VDJ sequences	This paper	GenBank: MF429952 - MF430833
Kappa chain Ig VJ sequences	This paper	GenBank: MF430834 - MF430850
Experimental Models: Cell Lines		
Human: FreeStyle 293F cell line	ThermoFisher Scientific	Cat#R79007
Human: HEp-2 cell line	ATCC	Cat#CCL-23
Experimental Models: Organisms/Strains		
Mouse: Aid-Cre^{ERT2} EYFP: AicdaCreERT2 flox-stop-flox-EYFP	(Dogan et al., 2009)	N/A
Mouse: PA-GFP: B6.Cg-*Ptprc*^{a} Tg(UBC-PA-GFP)1Mnz/J	The Jackson Laboratory	JAX: 022486

(*Continued on next page*)

Continued		
REAGENT or RESOURCE	SOURCE	IDENTIFIER
Mouse: TLR7$^{-/-}$: B6.129S1-*Tlr7*^{tm1Flv}/J	The Jackson Laboratory	JAX: 008380
Mouse: UBC-Cre^{ERT2}: B6.Cg-Tg(UBC-cre/ERT2)1Ejb/J	The Jackson Laboratory	JAX: 008085
Mouse: DTA: B6;129-*Gt(ROSA)26Sor*$^{tm1(DTA)Mrc}$/J	The Jackson Laboratory	JAX: 010527
Mouse: 564Igi: 564 HiKi	(Berland et al., 2006)	N/A
Mouse: Aid-Cre^{ERT2} Confetti: AicdaCreERT2-Rosa26Confetti	(Tas et al., 2016)	N/A
Oligonucleotides		
Primers for genotyping	This paper	Table S2
Primers for IgPCR	(Busse et al., 2014; Tiller et al., 2009)	Table S2
Sequences for Ig cloning	This paper	Table S3
Recombinant DNA		
Modified pVRC8400 vector for Ig cloning	(Kuraoka et al., 2016)	N/A
Software and Algorithms		
IgBLAST	(Ye et al., 2013)	https://www.ncbi.nlm.nih.gov/igblast/
CloAnalyst	(Kepler, 2013)	http://www.bu.edu/computationalimmunology/research/software/
CellProfiler	(Lamprecht et al., 2007)	http://cellprofiler.org/
ImageJ	Rasband WS, ImageJ, NIH, Bethesda, Maryland, USA	https://imagej.nih.gov/ij/
R	R Development Core Team (2008). R: A language and environment for statistical computing. R Foundation for Statistical Computing, Vienna, Austria.	https://www.r-project.org/
Other		
Antigens and control analytes used in autoantigen arrays	This paper	Table S1

CONTACT FOR REAGENT AND RESOURCE SHARING

Further information and requests for resources and reagents should be directed to and will be fulfilled by the Lead Contact, Michael C. Carroll (michael.carroll@childrens.harvard.edu).

EXPERIMENTAL MODEL AND SUBJECT DETAILS

Mice

C57BL/6J, B6.SJL (CD45.1), Photo-Activatable (PA)-GFP transgenic mice (Victora et al., 2010) (B6.Cg-Ptprca Tg(UBC-PA-GFP) 1Mnz/J), and TLR7 knockouts (B6.129S1-Tlr7tm1Flv/J) were obtained from Jackson Laboratories. AicdaCre^{ERT2} flox-stop-flox-EYFP mice (Dogan et al., 2009) were from Claude-Agnès Reynaud and Jean-Claude Weill (Institut Necker). The UBC-Cre^{ERT2} strain (B6.Cg-Tg(UBC-cre/ERT2)1Ejb/J) was kindly made available by Arlene Sharpe. The attenuated DTA line (B6;129-Gt(ROSA)26Sor < tm1(DTA)Mrc > /J) was kindly provided by Fred Alt (Boston Children's Hospital). 564Igi mice (Berland et al., 2006) were originally provided by Theresa Imanishi-Kari (Tufts University) and were maintained in-house. All mice were bred and maintained in the AAALAC-accredited facility at Harvard Medical School. AicdaCre^{ERT2}-Rosa26Confetti (Tas et al., 2016) donors were from Gabriel D. Victora (Whitehead Institute). Mice were specific pathogen-free (SPF) and maintained under a 12 hr light/dark cycle with standard chow diet. Both male and female mice were used. All animal experiments were conducted in accordance with the guidelines of the Laboratory Animal Center of National Institutes of Health. The Institutional Animal Care and Use Committee of Harvard Medical School approved all animal protocols (protocol numbers IS00000095 and IS00000111).

Cells

For the nucleolar purification protocol and for expression of IgG's, FreeStyle 293-F HEK cells were purchased from Invitrogen and grown in FreeStyle 293 Expression Medium at 37°C with 8% CO_2. For IF staining, HEp-2 cells were obtained from ATCC and cultured in EMEM containing 10% FBS at 37°C with 5% CO_2.

METHOD DETAILS

Antibodies and staining reagents

Commercial antibodies and staining reagents, from BioLegend: GL7-PacBlue, GL7-PE, GL7-A647, B220-PerCP-Cy5.5,αB220-APC-Cy7,αIgMb-FITC,αIgMa-PE, CD45.2-FITC, CD45.2-APC,αCD45.1-FITC,αCD45.1-PE, αIgD-PB,αCD21/35 (7E9)-PE, CD138-PE, CD38-PE-Cy7, CD31-A647, CD157-PE, Streptavidin-PE/Cy7; from eBioscience: CD95 (APO-1/Fas)-PE (clone 15A7) and viability dye Fixable live/dead stain Efluor780; from ThermoFisher Scientific: Rabbit-anti-Goat-A488, Hoechst 33342, DAPI (4',6-Diamidino-2-Phenylindole, Dihydrochloride), Phalloidin-A568; from Southern Biotech: AP-Goat-anti-Mouse IgG, AP-Goat-anti-Mouse IgG2a, AP-Goat-anti-Mouse IgG2c; from Rockland Immunochemicals: Rabbit polyclonal anti-B-Phycoerythrin; from DAKO: Rabbit polyconal anti-Mouse Immunoglobulins-biotin; from Perkin-Elmer: Europium-labeled streptavidin. In-house generated anti-idiotypic Ab, clone 9D11, conjugated to Alexa Fluor 647 or Alexa Fluor 568; in-house generated Rabbit polyclonal anti-C3b conjugated to Alexa Fluor 633.

Genotyping and FACStyping

Genotyping was performed using the primers and reaction conditions indicated in Table S1. For FACStyping mice were bled retroorbitally. Using heparinized capillary tubes, approximately 60-100 μl blood was drawn into Eppendorf tubes containing 30 μl acid-citrate-dextrose solution. Following collection, the stabilized blood was briefly spun down, then underlayered with 1 mL of Lymphocyte Separation Medium, and spun for 25 min, 1,600 RPM at RT. The mononuclear cell layer was aspirated and transferred into 1 mL ice-cold FACSbuffer, mixed, then pelleted at 200 *g* for 5 min. Cells were resuspended in FACSbuffer and processed for flow cytometric analysis as described further below. FACStyping of 564 mice was performed using B220, anti-IgMa, anti-IgMb, and 9D11. PA-GFP mice were FACStyped for PA-GFP positivity based on signal in the AmCyan/Pacific Orange channel.

Chimeras

Recipients were irradiated with 950 rad, then immediately placed on water containing antibiotics (sulfamethoxazole/trimethoprim) to prevent opportunistic infections during the reconstitution phase. Femurs and tibia were extracted from BM donors, mechanically cleaned and rinsed through several rounds of HBSS supplemented with 10 mM HEPES, pH 7.2, 1 mM EDTA and 2% heat-inactivated FBS (BM buffer). The bones were subsequently crushed in a mortar, and the cell extract was passed through a 70 μm cell strainer (Corning). An aliquot was subjected to RBC lysis and counted in a standard hemacytometer (Neubauer chamber). Based on cell counts, appropriate ratios of mixed BM were calculated to achieve final desired donor ratios. Cells were pelleted by centrifugation (200 *g*, 5 min) and resuspended at 1 * 10^8 cells per ml, and 100 μl was injected i.v. into each irradiated recipient ~10-12 hr post irradiation.

Additional procedures

To generate foreign-Ag-elicited GCs, mice were immunized intraperitoneally with 100 μg of chicken gamma globulin (Rockland Immunochemicals) precipitated in an equal volume of Imject Alum (ThermoScientific). Recombination of the Rosa26Confetti allele in Aid-Cre^{ERT2} mice was induced by a single gavage of 10 or 15 mg of tamoxifen (Sigma) dissolved in sunflower oil at 20 or 30 mg/ml. For in vivo-labeling of FDC networks, mice were injected intraperitoneally with 100 μg of rabbit polyclonal anti-B-PE (Rockland) two days prior to sacrifice, and subsequently intravenously with 10 μg B-PE (Molecular Probes/ThermoFisher) or 1 mg SA-PE-Cy7 (BioLegend) the day before sacrifice. Alternative FDC labeling approaches included i.v. injection of 10 μg A633-conjugated rabbit polyclonal-anti-C3b (in-house generated) or PE-conjugated anti-CD157 Ab (BioLegend) 1-2 days before sacrifice.

Mutiphoton imaging and photoactivation of explants

Spleen and LNs were harvested at different times post-immunization/tamoxifen. Adipose tissue was carefully removed under a dissecting microscope. Either thick transversal sections (~1 mm) were manually cut from spleens using surgical scissors, or longitudinal thick sections (~2-3 mm) were prepared by clamping the spleen between Styrofoam holders and manually slicing with a surgical scalpel. LNs and spleen sections were placed in FACS buffer (PBS, pH 7.2, 1 mM EDTA and 2% heat-inactivated FBS) in vacuum-grease chambers on microscope slides. Chambers were coverslipped and kept on ice before and immediately following imaging/photoactivation. All imaging was performed on an upright Olympus FV1200 MPE multiphoton system microscope fitted with either a 20X 0.95NA Plan water-immersion objective or a 25X 1.05NA Plan IR optimized water-immersion objective, a MaiTai HP DeepSee Ti-Sapphire laser (Spectraphysics), and 4 non-descanned detectors (2 GaAsP and 2 regular PMTs). Imaging of Confetti alleles was performed using λ = 940 nm excitation. Fluorescence emission was collected in three channels, using the following filter sets: a pair of CFP (480/40 nm) and YFP (525/50 nm) filters, separated by a 505 nm dichroic mirror, for CFP/GFP/YFP detection, and a third filter (605/70 nm) for RFP detection. Alexa 633-conjugated Ab was imaged using 830 nm excitation and a 665/40 nm emission filter. Imaging of PA-GFP explants was performed at λ = 930-940 nm, photoactivation was performed at λ = 830 nm. For live imaging, mice were anaesthetized using an isoflurane vaporizer, with 1.5%–2% isofluorane for the induction phase, followed by 0.5%–1% for maintenance. Adequate surgical plane of anesthesia was frequently verified throughout the procedure by testing the pedal withdrawal reflex. The mice were prepared using standard surgical technique.

Confetti analyses

Acquired stacks were rendered in Fiji (ImageJ). Counting was performed on 3-4 z planes from stacks acquired at 5 μm steps through the GC. Slices were at least 15-20 μm apart to preclude the possibility of double counting. Very sparse, < 50% occupation GC were discarded prior to analysis, as they were considered to harbor at least one expanded dark clone. Typically, greater than 250 GC B cells were quantified for a single GC per time point. Observers were blinded to animal status and inter-observer reliability was confirmed by independent counts of 15 GC with a concordance of more than 95% between 2 observers. Raw counts were converted to relative frequencies for each observable color to simplify analysis. Clonal dominance was calculated as the frequency of the most dominant clone/color at a given time point. Clonal divergence score was reported previously (Tas et al., 2016) and is calculated at a given time point by comparing the observed distribution of colors at time t to the expected frequencies resulting from random recombination. Expected frequencies for each of 10 possible colors was derived using explant data from day 3 post tamoxifen treatment where color distribution most closely mimics random recombination and prior to any selection events:

$$Clonal\ divergence\ score(t) = \sum_{i=1}^{10} \left| observedfreq_{color(i)} - expectedfreq_{color(i)} \right| .$$

Descriptors of GC behavior and clonality were graphed using GraphPad Prism 6.

Flow cytometry

Spleens and LNs were harvested into ice cold FACS buffer and mechanically dissociated using pestles in 1.5 mL Eppendorf tubes. Samples were filtered through 70 μm cell strainers (Corning) and spun down at ~200 *g* for 5 min. LN samples were resuspended in FACS buffer. Spleen samples were resuspended in RBC lysis buffer (155 mM NH_4Cl, 12 mM $NaHCO_3$, 0.1 mM EDTA), incubated for 2-3 min then spun down as before and resuspended in FACS buffer. Femurs and tibia were harvested, mechanically cleaned using coarse paper towels and placed into ice cold FACS buffer. Bones were processed by maceration in a mortar and the resulting BM cell suspensions were collected and passed through 70 μm cell strainers. BM cell suspensions were spun down and subjected to RBC lysis as for the spleen, then spun again and resuspended in FACS buffer. Peyer's patches were snipped off the outer surface of the small intestine, collected into ice cold FACS buffer and subsequently washed through 5-10 changes of FACS buffer to remove contaminating fecal matter. Peyer's patches were then mechanically dissociated using pestles in 1.5 mL Eppendorf tubes as for the spleens and LNs, filtered through 70 μm cell strainers, spun down and finally resuspended in FACS buffer. Samples were added to wells of 96-well round-bottom plates, spun down and resuspended in 100 μl staining mix (appropriate Ab and viability dye cocktail in FACS buffer). Staining was performed for 30 min on ice, followed by addition of 150 μl wash buffer. Plates were subsequently centrifuged 200 *g* for 5 min, and supernatants flicked out of the plates. For two-step staining procedures secondary staining mix was added (appropriate secondary Ab mix and viability dye in FACS buffer), and the process repeated. Following the last wash, samples were resuspended in 200 μl FACS buffer and transferred to FACS tubes. Flow cytometric analyses were performed on one of 3 different instruments (BD Biosciences), depending on the experiment: a four color, six parameter FACSCalibur equipped with 488 nm and 633 nm lasers; a standard 3 lasers-configuration (405 nm, 488 nm and 633 nm) FASCSCanto2, with 8-color and 10 parameter analytical capabilities; and a 5-laser, 20-parameter FACSAria 2 SORP (lasers: 355 nm, 488 nm, 633 nm, 405 nm, 594 nm) equipped with a PMT option for FSC, enhanced optics and digital focusing and a 300 mW 488 nm laser from Coherent.

Bulk sequence analysis

Cell suspensions were stained as for flow cytometry, washed, and resuspended in FACS buffer. Bulk sort was performed on a 5-laser FACSARIA II Special Order system (355, 405, 488, 640, 594 nm laser lines; FCS-PMT module and enhanced optics and digital focusing), using a single-cell sort mask. Cells were sorted directly into RNA lysis buffer (Zymo Research) in FACS tubes, spun down briefly following completion of collection, and frozen at −80°C until further processing. RNA was purified using the Zymo Quick RNA Miniprep kit (Zymo Research) following the manufacturer's instructions, and RNA yields determined using a NanoDrop1000. Complementary DNA was generated using M-MLV Reverse Transcriptase (ThermoFisher Scientific) at standard conditions. Amplification of V(D)J segments was performed using consensus primers based on Tiller et al. (2009), and Busse et al. (2014), (see also Table S1) and GoTaq DNA polymerase (Promega) under the conditions described herein. Amplicons were TOPO-TA cloned into the pCR2.1-TOPO vector and used for transformation of DH5α, which were subsequently plated on LB-agar containing kanamycin, X-gal and IPTG. Following incubation overnight at 37°C, single defined white colonies were picked into 10 μl of autoclaved distilled water. From each sample, 1 μl was used as input for amplicon PCR using M13 Forward and Reverse primers and GoTaq DNA polymerase. From 20 μl reactions, 2-5 μl were run on analytical agarose gels, and the remainder was precipitated by addition of 1/10th volume 3 M sodium acetate (pH 5.2) and 2.5 volumes 96% ethanol. Following overnight incubation at −20°C, samples were spun at 3,500 rpm for 30 min, the supernatant flicked off, and the pellet washed with 96% ethanol. Pellets were subsequently dried and resuspended in 12 μl 10 mM Tris buffer, pH 8.5. Nucleic acid concentration and purity was measured on NanoDrop1000, and samples were submitted to sequencing at the DFCI Sequencing Core using either T7 or M13 Reverse primer. Sequence traces were oriented with V(D)J in forward orientation and truncated based on the msVHE and mu- or gamma-inner primer sequences. Files were imported into CLC Sequence Viewer 7, the resulting sequences extracted and grouped, then exported as sequence lists in fasta format. Sequences were submitted to IgBlast against the full NCBI V(D)J dataset with standard settings (Ye et al., 2013). Output was imported

into Microsoft Excel, filtered to include only full-length sequences, then tabulated using the PivotTable function. Resulting VH segment usage and mutation tables were rendered in GraphPad Prism 6.

Single cell sequence analysis

Cell suspensions were stained as for flow cytometry, washed, and resuspended in FACS buffer. Single cell sort was performed on a 5-laser FACSARIA II Special Order system (355, 405, 488, 640, 594 nm laser lines; FCS-PMT module and enhanced optics and digital focusing), using a single-cell sort mask. Single cells were sorted directly into wells of 96-well semi-skirted PCR plates containing 5 μl buffer TCL (QIAGEN) supplemented with 1% beta-mercaptoethanol. Following collection, plates were sealed with PCR tape, spun briefly, and immediately placed at −80°C. Plates were processed separately in a laminar flow hood following wipe-down and UV illumination. All reagents were prepared fresh for each experiment, based on pre-aliquots and stock solutions. Plates were thawed on ice, and to each well was added 2.2 vol. RNA-SPRI beads (11 μl per well, Agencourt RNAClean XP). Samples and beads were mixed well by pipetting, followed by incubation 10 min at RT. The plates were then incubated 5 min on a plate magnet, and the supernatant was removed using an 8x multichannel and following the direction of the magnet. Beads were washed 3 times with 100 μl 80% EtOH, in each round by displacing and repositioning wells from one magnet bar to a neighboring one several times. Washed beads were air-dried for 10 min, and RNA was eluted in 4.5 μl of Mix1 (1.1 μM anchored Oligo-dT, 2.2 mM dNTP, and 1.1 U/μl of RNaseOut) per well by dispensing it directly over the beads and by pipetting up and down. Plates were spun briefly, incubated 3 min at 72°C, followed by 1 min on ice, then to each well was added 5.5 μl of Mix2 (1.8 U/μl RNaseOUT, 3.6 U/μl Maxima H- Reverse Transcriptase, 0.9 M Betaine, 5.5 mM $MgCl_2$, and containing 2 μl 5x RT buffer per reaction). Plates were again spun briefly, and RT reactions were then run on a thermocycler, 50°C for 1h, 4°C hold. For PCRs, again all reagents were prepared fresh for each experiment, based on pre-aliquots and stock solutions. The 10 μl cDNA reactions were diluted 5-fold with 40 μl autoclaved MilliQ water, and from this 5 μl was used per 20 μl 1^{st} round PCR reaction. From the 1^{st} round PCR, 1 μl was used as input for 2^{nd} round (semi-nested) PCR reaction. Primers and PCR conditions were as described above for the bulk sequence analysis. Amplicons were precipitated and analyzed as described, then sent for sequencing using Mu-inner and Gamma-inner, for mu and gamma heavy chain amplicons respectively. Sequence traces were oriented with V(D)J in forward orientation and truncated based on the msVHE primer sequence. Files were imported into CLC Sequence Viewer 7, the resulting sequences extracted and grouped, then exported as sequence lists in fasta format. Sequences were submitted to IgBlast against the full NCBI V(D)J dataset with standard settings (Ye et al., 2013). Output was imported into Microsoft Excel, filtered to include only full-length sequences, then tabulated using the PivotTable function. Resulting VH segment usage and mutation tables were rendered in GraphPad Prism 6.

Clonal lineage determination and inference

The program Cloanalyst (Kepler, 2013) was used to annotate isolated paired heavy-light VDJ/VJ sequences, and to infer intermediates and the unmutated common ancestor (UCA). The phylogenetic tree of the clonal lineages was then reconstructed.

Cloning, expression and purification of IgGs

The 38 genes encoding the Ab V_H, V_L and the UCA were synthesized (Integrated DNA Technologies) and cloned into the modified pVRC8400 vector between a tissue plasminogen activation (TPA) signal sequence and the constant domains of the mouse IgG1 C_{H1}-C_{H3} and C_L (Kuraoka et al., 2016). Mouse IgG1,k were produced by transient transfection of 293T adapted for suspension culture, using polyethylenimine (PEI, Polysciences) as the transfection reagent. The supernatant was harvested 6 days after transfection and clarified from cellular debris by centrifugation at 4,200 rpm for 20 min. IgGs were purified using Protein G agarose (Thermo) and dialyzed in PBS. Purified IgGs were concentrated and stored at 4°C until needed.

Nucleolar ELISA/TRIFMA

Nucleoli were purified from cultured HEK293F FreeStyle cells (Invitrogen). The cells were grown to a density of ~1 * 10^6 cells per ml, spun down and resuspended in fresh pre-warmed medium the day before, and on the day of isolation added 1/10 volume fresh medium 1 hr before commencement of the protocol. For the isolation, ~10^8 cells were spun down at ~200 *g* (~1000 rpm, Beckman GS-6 centrifuge, GH-3.8 rotor) for 5 min, the supernatant decanted, and they were resuspended in 5 mL ice-cold Buffer A (10 mM HEPES, pH 7.9, 10 mM KCl, 1.5 mM $MgCl_2$, 0.5 mM DTT). After incubation on ice for 5 min, the cells were transferred to a pre-cooled 7 mL Dounce homogenizer (Wheaton Scientific) and subjected to 10 strokes using a tight pestle (“A” specification: 0.0010” - 0.0030” clearance), while keeping the homogenizer on ice. An aliquot of the homogenate was checked under a phase contrast microscope, and the procedure repeated as necessary, until > 90% of the cells were burst, leaving intact nuclei, with various amounts of cytoplasmic material attached. The homogenate was then centrifuged 200 *g* for 5 min at 4°C. Following aspiration of the supernatant, the pellet, containing enriched but not highly pure nuclei, was resuspended in 3 mL S1 solution (0.25 M Sucrose, 10 mM $MgCl_2$). The resuspended pellet was layered over 3 mL of S2 solution (0.35 M Sucrose, 0.5 mM $MgCl_2$) and centrifuged at ~1,400 *g* (2,500 rpm) for 5 min at 4°C. The pellet was resuspended in 3 mL of S2 solution and the resulting nuclear suspension was sonicated for 6 × 10 s bursts (with 10 s rest intervals between each burst) using a Misonix XL 2020 sonicator fitted with a microtip probe, and set at power setting 5. The sonicated nuclei were periodically checked under a phase contrast microscope to ensure the virtual absence of intact cells and nuclei, and confirm the presence of free nucleoli observable as dense refractile bodies. The sonicated sample was layered over 3 mL of S3 solution (0.88 M Sucrose, 0.5 mM $MgCl_2$) and centrifuged at 3,000 *g* (3,500 rpm) for 10 min at 4°C.

The nucleoplasmic fraction was aspirated and the nucleolar pellet was resuspended in 0.5 mL of S2 solution, followed by centrifugation at 1,430 *g* (2,500 rpm) for 5 min at 4°C and resuspension in 0.5 mL of S2 solution. Each batch was checked carefully under a phase contrast microscope to ensure presence of highly purified nucleoli without any other material, and stored at −80°C until use. For quantification of nucleoli 10-fold dilution series were prepared and loaded in a standard hemacytometer, allowed to settle, and then counted using phase-contrast. We routinely obtained approximately ~10^8 nucleoli, i.e., 1 nucleolus per 1 cell input, indicating a recovery of 25%–33% (on average 3-4 nucleoli per HEK293F cell), and we occasionally observed partially intact nuclei or fragments hereof (around 1/40 to 1/50), indicating a purity of > 97.5%. Fluoronunc microtiter plates were added nucleoli, 2 × 10^6/ml in PBS, 100 μl per well, spun at 2,500 rpm (~1,300 g), 10 min at 4°C, then left to coat overnight at 4°C. Wells were emptied and blocked by incubation with BSA, 1 mg/ml PBS, for 1 hr at RT. Plates were washed three times with TBS/Tw (10 mM Tris-HCl, 145 mM NaCl, pH 7.4, containing 0.05% v/v Tween-20), then added standard, controls and samples: standard, 564 C11 mAb in sqrt10 dilution series from ~4000 ng/ml to ~3.9 ng/ml, plus "0" (buffer only); samples and controls, serum diluted 1/100; all in duplicate, 100 μl per well in TBS/Tw, incubated 2 hr at RT, then washed 3x with TBS/Tw. This was followed by incubation with secondary AP-conjugated Ab (total IgG, IgG2a, IgG2c, all from Southern Biotech), 1/2,000 in TBS/Tw, 100 μl/well, for 1 hr at RT. Finally, wells were washed 3 x with TBS/Tw and developed with phosphatase substrate, 1 mg/ml AP substrate buffer (1 M diethanolamine, pH 9.8, with 0.5 mM $MgCl_2$), reading out on a SPECTRAmax 340 Microplate Reader running SoftMax Pro v. 5.4. In a time-resolved immunofluorometric assay (TRIFMA) variation of the assay, two-step development was performed by adding in-house biotiniylated rabbit anti-mouse IgG Ab (DAKO) followed by Eu^{3+}-labeled streptavidin (0.1 mg/ml in TBS/Tw containing 25 μM EDTA). After the final wash, enhancement solution (Perkin-Elmer) was added and time-re- solved fluorescence was read on a Victor3 (Perkin-Elmer).

Immunofluorescence confocal microscopy

Freshly harvested tissue was embedded in OCT (TissueTek) and immediately frozen at −80°C. Tissue blocks were equilibrated at cutting temperature (−16 to −20°C depending on tissue type) and 6-10 μm thick sections were cut on a cryostat. Tissue sections were mounted on SuperFrost+ slides (Fisher Scientific) and fixed using either ice-cold acetone or freshly thawed 4% PFA, for 5-10 min. PFA-fixed slides were incubated with TBS to block residual primary amine reactivity. Slides were then rinsed with PBS and incubated with block/perm buffer (PBS, 2% FBS, 0.1% NaN_3, and 0.1% Triton X-100) for 30 min. This was followed by incubation with primary Ab mixture in staining buffer (PBS, 2% FBS, 0.1% NaN_3), overnight at 4°C. For two step staining procedures, the slides were washed 3 times with PBS, 0.01% Tween-20, then added secondary Ab mixture in staining buffer, and incubated for 2 hr at RT. At the end of either one- or two-step staining procedures, slides were washed once with staining buffer for 5 min, then 3 times 5 min with PBS, 0.01% Tween-20. Slides were spot-dried, then mounted in Fluoro-Gel (Electron Microscopy Sciences) and coverslipped. Imaging was performed using a Fluoview FV1000 inverted Olympus IX 81 confocal microscope, equipped with 6 laser lines (405, 457, 488, 515, 559, 635 nms) and 4 fluorescence + 1 transmission detector (PMTs).

HEp-2 Immunofluorescence assay

HEp-2 cells (ATCC) were split 1/3 in T175 on day −2 and seeded to glass coverslips at day −1 (100K/well, 24 well). Cells were fixed with 1%PFA for 20 min at RT. Cells were then blocked and permeabilized with block/perm buffer (2% FBS, 0.1% Tx-100 in PBS). After 30 min, cells were stained o/n in block/perm buffer with indicated antibodies at 10 ug/ml, 1 ug/ml or 0.1 ug/ml (C11 and 564 only). The next day, coverslips were washed 3 times and incubated for one hour with Goat anti Mouse IgG (H+L) Alexa488 (Life Technologies), phalloidin Alexa568 (Life Technologies) and DAPI. Coverslips were then washed 4 times and mounted on slides with Fluorogel as mounting medium. Detectors were set to no primary Ab control. Anti HA Ab 6649 was used as negative control. C11, the original hybridoma from which the 564 BCR was created was used as positive control in addition to re-cloned 564.

Image analysis

Images were quantified using CellProfiler (Lamprecht et al., 2007). For kidney sections, glomerulus specific masks were generated based on CD31 signal and the mean pixel intensity was measured within each mask. For HEp-2 slides, quantifications were done based on the DAPI (nucleus) and Phalloidin staining. Cell outlines were detected using the phalloidin staining and as a function of the detected nuclei. A cytoplasmic mask was generated by subtracting the nucleus mask from the cell mask. Each bar represents a mean of individual objects (for instance a mean of MFI from 20 nuclei).

Autoantigen arrays

Autoantigen arrays were generated and assays on the arrays were performed as described previously (Ayoglu et al., 2016). Unless stated otherwise in Table S3, 6 μg of each Ag and a three-point dilution series of control mouse and anti-mouse antibodies (0.25, 1, 4 μg) were diluted in PBS and transferred into 3 × 96-well plates. Analytes were coupled to 1x10^6 carboxylated magnetic beads per ID (MagPlex-C, Luminex Corp.). Beads were distributed into 3 × 96-well plates (Greiner BioOne), washed and re-suspended in phosphate buffer (0.1 M NaH_2PO_4, pH 6.2) using a plate washer (Biotek). Bead surface was activated by addition of 100 μL of phosphate buffer containing 0.5 mg of 1-ethyl-3(3-dimethylamino-propyl)carbodiimide (Pierce) and 0.5 mg N-hydroxysuccinimide (Pierce). After 20 min incubation on a shaker (Grant Bio), beads were washed and re-suspended in activation buffer (0.05 M MES, pH 5.0). Diluted Ags and control antibodies were incubated with beads for 2 hr at RT. The beads were washed 3 × in 100 μl PBS-T, re-suspended in 60 μl storage buffer (Blocking reagent for ELISA, Roche) and stored in plates at 4°C overnight. Immobilization of the Ags were

confirmed and the assay conditions were optimized by analysis of several mouse monoclonal antibodies, such as anti-La/SSB (Santa Cruz), anti-Ro52 (Santa Cruz), anti-His6 tag (Invitrogen), anti-Scl70 (Immunovision), anti-SSB (Immunovision), anti-IL17A (eBiosciences), and a rabbit polyclonal Ab, anti-H2b (abcam), all at 1 μg/ml (data not shown). In addition, dilution series (1:50 to 1:300) of various autoimmune disease state human plasma for ds-DNA, Scl-70, SSA, SSB, cardiolipin, whole histones and RNP (Immunovision), as well as normal human sera (Immunovision) and previously in-house characterized MRL/lpr sera pool and BALB/c sera pool were used to optimize the assay conditions prior to analysis (data not shown).

Based on the optimized assay conditions, the mouse sera were diluted 1:60 in an assay buffer of 0.05% PBS-T supplemented with 3% (w/v) BSA (Sigma) and 5% (w/v) blotting-grade nonfat dry milk (BioRad) and transferred into a 96-well plate. The bead array was distributed into a 384-well plate (Greiner BioOne) by transfer of 5 μl bead array per well. Using a liquid handler (SELMA, CyBio), 45 μl of the 1:60 diluted sera were aliquoted and transferred into each of the three different quadrants of a 384-well plate. Samples were incubated for 90 min on a shaker (Grant Bio) at RT. The beads were washed with 3 × 60 μl PBS-T on a plate washer (EL406, Biotek). Using a liquid handler (SELMA, CyBio), 50 μl of R-PE conjugated Fcγ fragment specific goat anti-mouse IgG (Jackson), R-PE conjugated Fcγ subclass 2a specific goat anti-mouse IgG (Jackson) and R-PE conjugated Fcγ subclass 2c specific goat anti-mouse IgG (Jackson) were transferred to the three different quadrants of the 384-well plate, allowing for a parallel detection different isotypes. All secondary antibodies were diluted 1:500 in a buffer consisting of 3% BSA in 0.05% PBS-T. After incubation with the secondary antibodies for 45 min, the plate was washed with 3 × 60 μl PBS-T and re-suspended in 60 μl PBS-T for readout in a FlexMap3D instrument (Luminex Corp.). Cloned antibodies were analyzed following the same protocol, where all the antibodies were diluted to 20 μg/ml in 3% (w/v) BSA and detected with the 1:500 diluted R-PE conjugated Fcγ fragment specific goat anti-mouse IgG (Jackson). At least 100 events per bead ID were counted and binding events were displayed as median fluorescence intensity (MFI). Data was analyzed using R (R Development Core Team, 2008). Heatmaps were rendered using the pheatmap package following log2-transformation.

QUANTIFICATION AND STATISTICAL ANALYSIS

All statistical analyses were performed in GraphPad Prism version 6, as defined throughout the text and figure legends.

DATA AND SOFTWARE AVAILABILITY

The data presented in this manuscript are tabulated in the main paper and in the STAR Methods. The sequences used for production of recombinant antibodies are compiled in Table S2. The accession numbers for the heavy chain Ig VDJ sequences reported in this paper are GenBank: MF429952–MF430833. The accession numbers for the Kappa chain Ig VJ sequences reported in this paper are GenBank: MF430834–MF430850.

Supplemental Figures

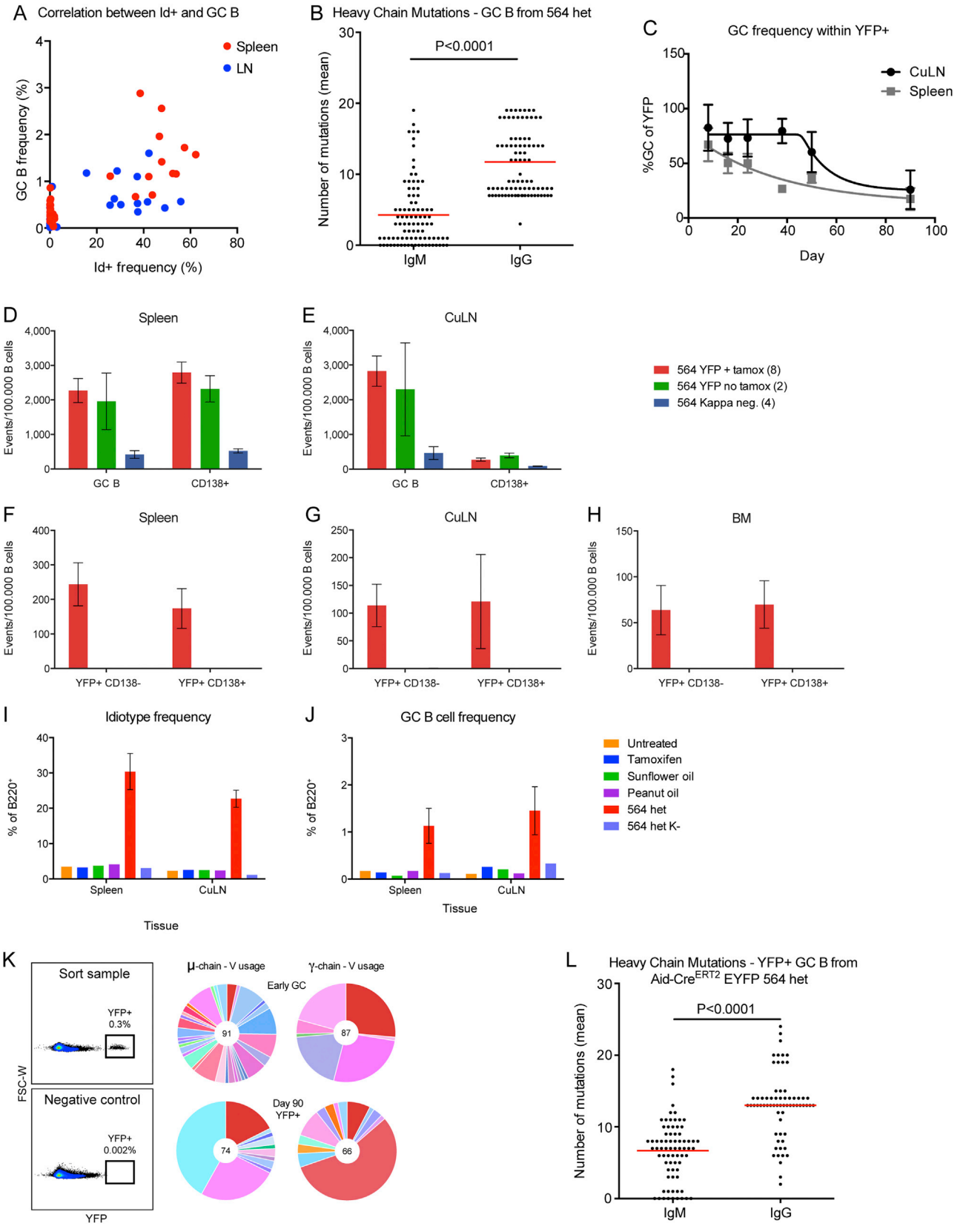

(legend on next page)

Figure S1. Correlation Analysis of Id$^+$ and GC Frequencies, Mutation Analyses, and Basic Characterization of the 564Igi Aid-Cre^{ERT2} EYFP Reporter, Related to Figure 1

(A) Correlation plot for Id+ cell frequency versus GC B cell frequency in spleen or cutaneous LN, across the cohort presented in Figures 1A–1C. Each dot represents one mouse, for a total of 34 mice analyzed.

(B) Mutation analysis for the heavy chains (IgM or IgG) of bulk-sorted GC B cells from two heterozygous 564Igi mice. Each dot represents one heavy chain. The mean number of mutations is indicated. p value given for two-tailed Mann-Whitney test.

(C) GC B cell frequency measured within the YFP$^+$ population for the cohort shown in Figures 1H–1L. Mean ± SEM is shown for 6 (Day 8, 16, 24), 2 (Day 38 and 50) and 3 (Day 90) mice from 3 independent cohorts.

(D) Total GC B and CD138+ (plasma) cells in spleen of tamoxifen pulsed 564 Aid-Cre^{ERT2} EYFP (n = 8), non-pulsed 564 Aid-Cre^{ERT2} EYFP (n = 2) and 564 K- controls (n = 4). Mean ± SEM is given.

(E) as in (D), but for cutaneous LN.

(F) Frequencies of YFP$^+$CD138$^-$ (GC and memory) and YFP$^+$CD138$^+$ (plasma) cells in spleen of the cohort represented in (D).

(G) As in (F), but for cutaneous LN.

(H) As in (F), but for BM.

(I) Id frequencies of untreated, tamoxifen in sunflower oil-treated, sunflower oil only treated, and peanut oil-treated B6, as well as untreated 564het and 564het K- mice (n = 1 per group, except for 564het with n = 2, mean ± SEM).

(J) GC B cell frequencies of the same cohort as in (I).

(K) FACS plots showing the frequency of YFP$^+$ cells in a Day 90 tamoxifen pulsed 564Igi Aid-Cre^{ERT2} EYFP mouse (top panel) versus a negative control (bottom panel). Results of sequencing of the mu-chain (left) and gamma chain (right) of FACS sorted GC cells of 564Igi mice (top) and Day 90 tamoxifen pulsed 564Igi Aid-Cre^{ERT2} EYFP mice (bottom).

(L) Mutation analysis for the heavy chains (IgM or IgG) of bulk-sorted YFP$^+$ cells from two Day 90 tamoxifen pulsed 564Igi Aid-Cre^{ERT2} EYFP mice. Each dot represents one heavy chain. The mean number of mutations is indicated. p value given for two-tailed Mann-Whitney test.

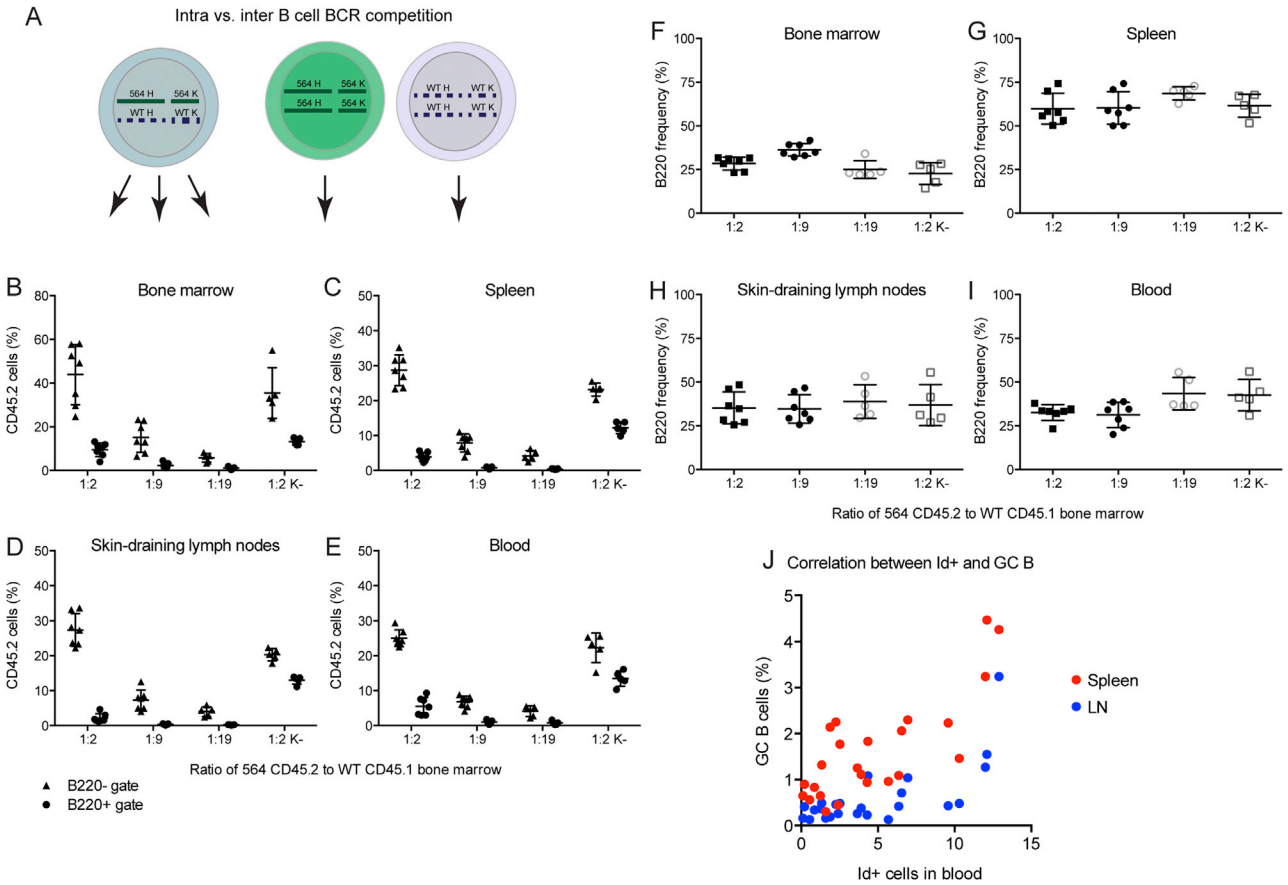

Figure S2. Illustration of Intra- versus Inter-B-Cell BCR Competition and Basic Characterization of the 564Igi Mixed Chimera Model, Related to Figure 2

(A) Illustration of conceptual difference between intra- and inter-B cell BCR competition occurring in 564hets and 564 mixed BM chimeras, respectively. In the 564hets, "WT cells" arise through inactivation of the 564 locus and rearrangement of the endogenous Ig locus. In the mixed chimeras, use of 564 homozygous donors "locks in" the 564 cell fate, whereas the wild-type repertoire is entirely normal.

(B) CD45.2 (564 BM-derived) cell frequencies in the $B220^{-}$ (triangles) and the $B220^{+}$ (circles) population of the lymphocyte gate in BM of 564 CD45.1 mixed chimeras. Mean ± SD are also indicated.

(C) As (B), but for spleen.

(D) As (B), but for skin-draining LN.

(E) As (B), but for blood.

(F) $B220^{+}$ cell frequencies in the lymphocyte gate in BM of 564 CD45.1 mixed chimeras. Mean ± SD are also indicated.

(G) As (F), but for spleen.

(H) As (F), but for skin-draining LN.

(I) As (F), but for blood.

(J) Correlation plot for Id+ cell frequency versus GC B cell frequency in spleen or cutaneous LN, across the cohort presented in Figure 2. Each dot represents one mouse, for a total of 24 mice analyzed.

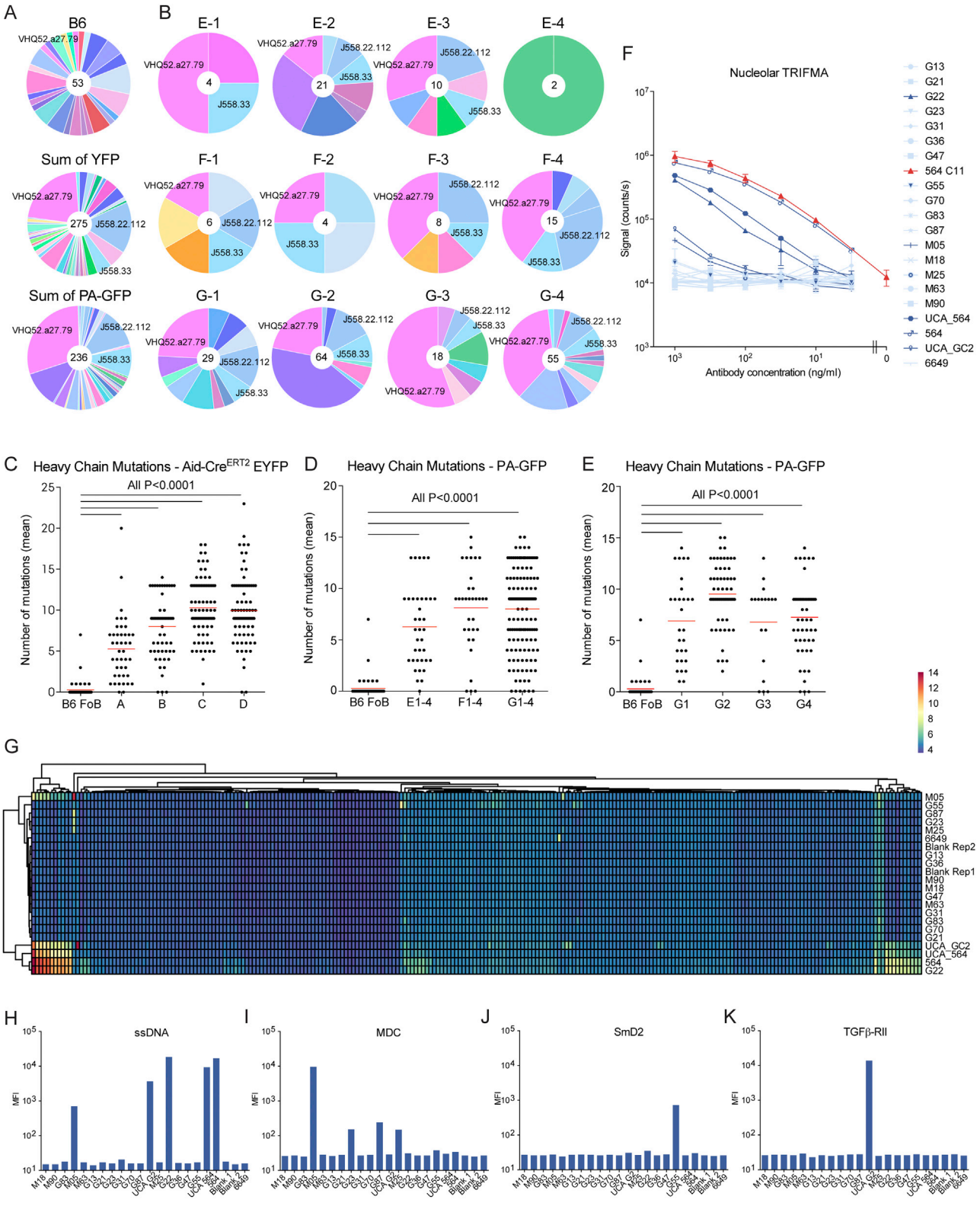

Figure S3. Heavy Chain V Segment Usage, Mutation Analyses, and Autoantigen Array Profiling of Cloned Antibodies, Related to Figure 3

(A) Heavy chain V segments observed in B6, sum of all YFP, and sum of all PA-GFP, clones. Colors congruent with Figure 3.

(B) Heavy chain V segments observed in 4 GC of 3 independent mice analyzed. Colors congruent with Figure 3.

(legend continued on next page)

(C) Mutation analysis for the heavy chains (IgM and IgG) of single-sorted YFP$^+$ GC B cells from 4 different (A-D) Aid-Cre^{ERT2} EYFP WT 564Igi mixed chimeras. Each dot represents one heavy chain. The mean number of mutations is indicated. p value given for Kruskal-Wallis test with Dunn's posttest comparing to naive follicular B cells from B6.

(D) Mutation analysis for the heavy chains (IgM and IgG) of single-sorted photoactivated GC B cells of 4 GC (1-4) of 3 different (E-G) PA-GFP WT 564Igi mixed chimeras. Each dot represents one heavy chain. The mean number of mutations is indicated. p value given for Kruskal-Wallis test with Dunn's posttest comparing to naive follicular B cells from B6.

(E) Mutation analysis for the heavy chains (IgM and IgG) of single-sorted photoactivated GC B cells of 4 GC (1-4) of one (G) of the PA-GFP WT 564Igi mixed chimeras. Each dot represents one heavy chain. The mean number of mutations is indicated. p value given for Kruskal-Wallis test with Dunn's posttest comparing to naive follicular B cells from B6.

(F) Results of nucleolar TRIFMA titrations of cloned antibodies from Figure 3. Positive or borderline antibodies from HEp-2 screen are indicated in dark blue or mixed, while negative antibodies are in light blue. The positive control, hybridoma-derived 564 C11, is displayed in red.

(G) Clustered, unscaled heatmap of autoAg reactivities of cloned antibodies from Figure 3. Clone identity is indicated on the righthand side. Identity of individual Ags from left to right is indicated in Table S3. The scale is indicated in the top righthand corner.

(H) Bar graph representation of data from (G) for ssDNA reactivity.

(I) Bar graph representation of data from (G) for MDC reactivity.

(J) Bar graph representation of data from (G) for SmD2 reactivity.

(K) Bar graph representation of data from (G) for TGFβ-RII reactivity.

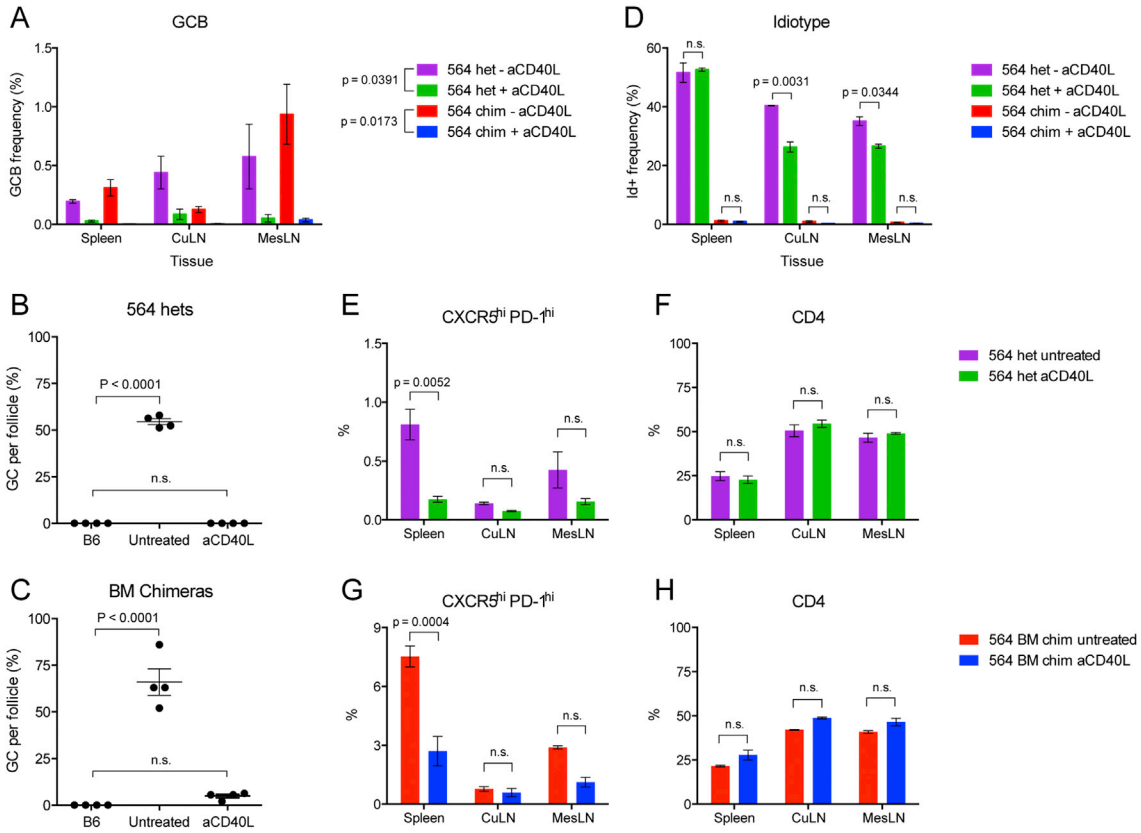

Figure S4. T Cell Dependence and Analysis of T Follicular Helper Cells in the 564Igi and 564Igi Mixed Chimera Models, Related to Figure 4

(A) GC B cell frequencies across spleen, cutaneous LN and mesenteric LN of untreated versus anti-CD40L Ab treated heterozygous 564Igi mice and 564 mixed BM chimeras. Mean ± SEM is given for 2 mice per group. Multiplicity-adjusted p values for two-way ANOVA with Tukey's posttest.

(B) Frequencies of GC per follicle as quantified by confocal IF analysis of spleen sections from treated versus untreated heterozygous 564Igi mice. Mean ± SEM is indicated. Multiplicity-adjusted p values given for one-way ANOVA with Dunnett's posttest.

(C) As in (B), but for 564 mixed chimeras.

(D) As in (A), but showing Id frequencies. p values given for two-way ANOVA with Sidak's posttest.

(E) Tfh ($CXCR5^{hi}PD\text{-}1^{hi}$) cells in spleen, skin-draining LN and mesenteric LN of untreated and CD40L-treated heterozygous 564Igi mice. p values given for two-way ANOVA with Sidak's posttest.

(F) As in (E), but showing CD4 T cell frequencies.

(G) As in (E), but for 564 mixed chimeras.

(H) As in (E), but showing CD4 T cell frequencies for 564 mixed chimeras.

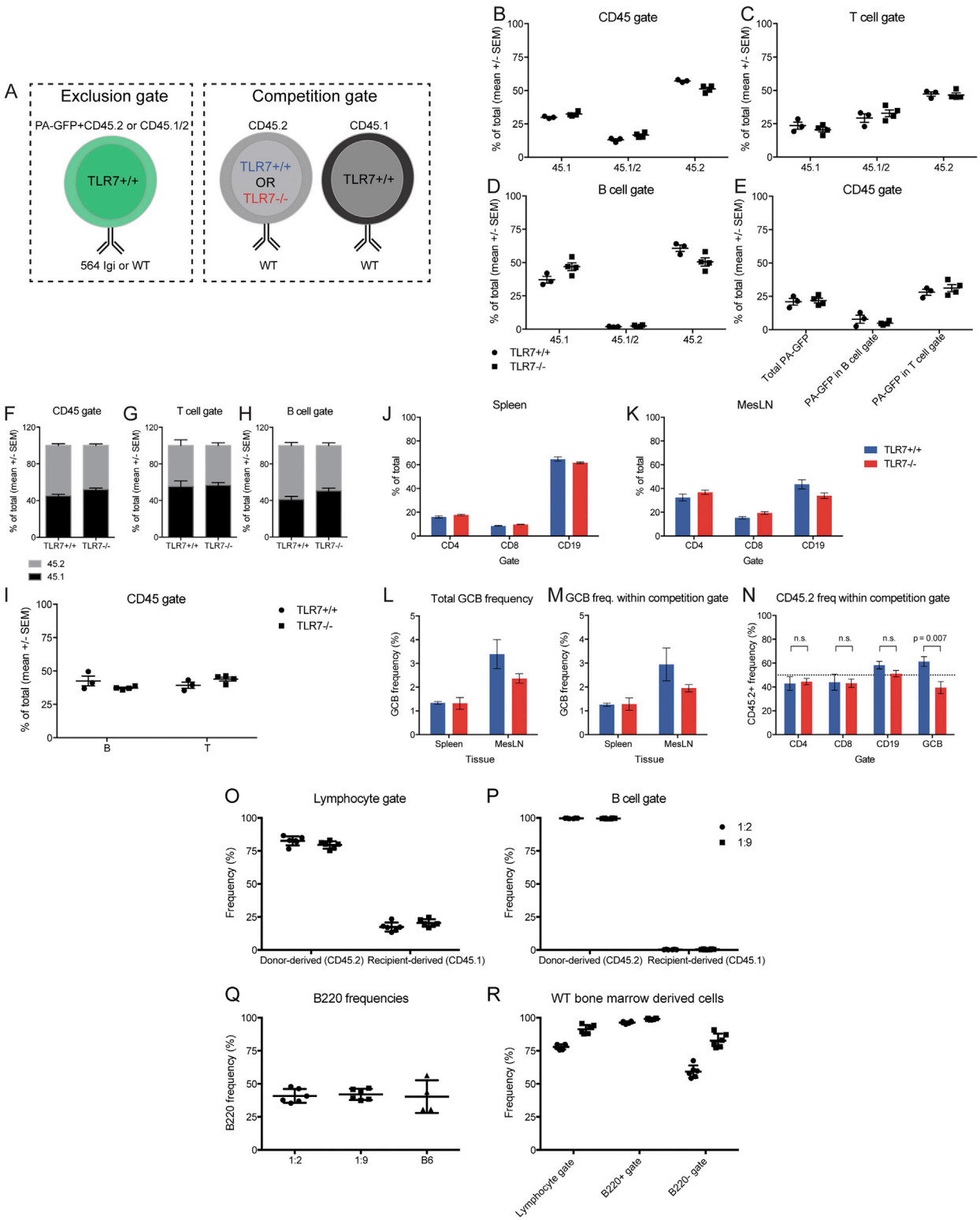

Figure S5. Schematic Overview and Basic Characterization of 564Igi TLR7$^{-/-}$ Mixed Chimeras, and Basic Characterization of 564Igi DTA Mixed Chimeras, Related to Figure 4

(A) Schematic overview of exclusion and competition gates in the experiment, with indication of the different compartments, their congenic markers and BCR identities.

(legend continued on next page)

(B) Total frequencies of 45.1 positive, 45.1/2 double positive, and 45.2 positive cells (as indicated on the x axis) within the CD45 gate in blood of 564 TLR7$^{+/+}$ (circles) or 564 TLR7$^{-/-}$ (squares) chimeras. Mean ± SEM is indicated.
(C) As in (B), but for the T cell gate.
(D) As in (B), but for the B cell gate.
(E) PA-GFP+ (564 BM-derived) cell frequencies within the total lymphocyte gate, the B cell gate, and the T cell gate (as indicated on the x axis) within the CD45 gate in blood of 564 TLR7$^{+/+}$ (circles) or 564 TLR7$^{-/-}$ (squares) chimeras. Mean ± SEM is indicated.
(F) Relative frequencies of CD45.1 and CD45.2 cells in the CD45 gate, within the competition gate, in blood of 564 TLR7 mixed chimeras. Mean ± SEM is shown.
(G) As in (F), but for the T cell gate.
(H) As in (F), but for the B cell gate.
(I) Total B and T cell frequencies in blood of 564 TLR7$^{+/+}$ (circles) and 564 TLR7$^{-/-}$ (squares) mixed chimeras. Mean ± SEM is indicated.
(J) Total splenic CD4, CD8 and CD19 frequencies (as indicated on the x axis) within the lymphocyte gate for 564 TLR7$^{+/+}$ (blue) and 564 TLR7$^{-/-}$ (red) mixed chimeras. Mean ± SEM is shown.
(K) As in (J), but for mesenteric LN.
(L) Total GC B frequencies in spleen and mesenteric LN.
(M) GC B frequencies within the competition gate.
(N) CD45.2 frequencies within the competition gate for CD4, CD8, CD19 and GCB populations (as indicated on the x axis) in mesenteric LN. Mean ± SEM shown, with multiplicity adjusted p values for two-way ANOVA using Sidak's posttest. The dotted line indicates the expected 50% frequency.
(O) Frequency of donor-derived (CD45.2) versus recipient derived (CD45.1) cells within the lymphocyte gate in blood of 1:2 (circles) and 1:9 (squares) 564 DTA chimeras. Mean ± SD is indicated.
(P) Similar to (O), but for the B cell subgate.
(Q) B220 frequencies in 1:2 and 1:9 564 DTA chimeras, compared to B6 mice. Mean ± SD is indicated.
(R) Frequency of PA-GFP+ (WT BM-derived) cells after exclusion of recipient-derived CD45.1+ cells, within the lymphocyte gate, B220+ gate and B220- gate of 1:2 (circles) and 1:9 (squares) 564 DTA mixed chimeras. Mean ± SD is indicated.

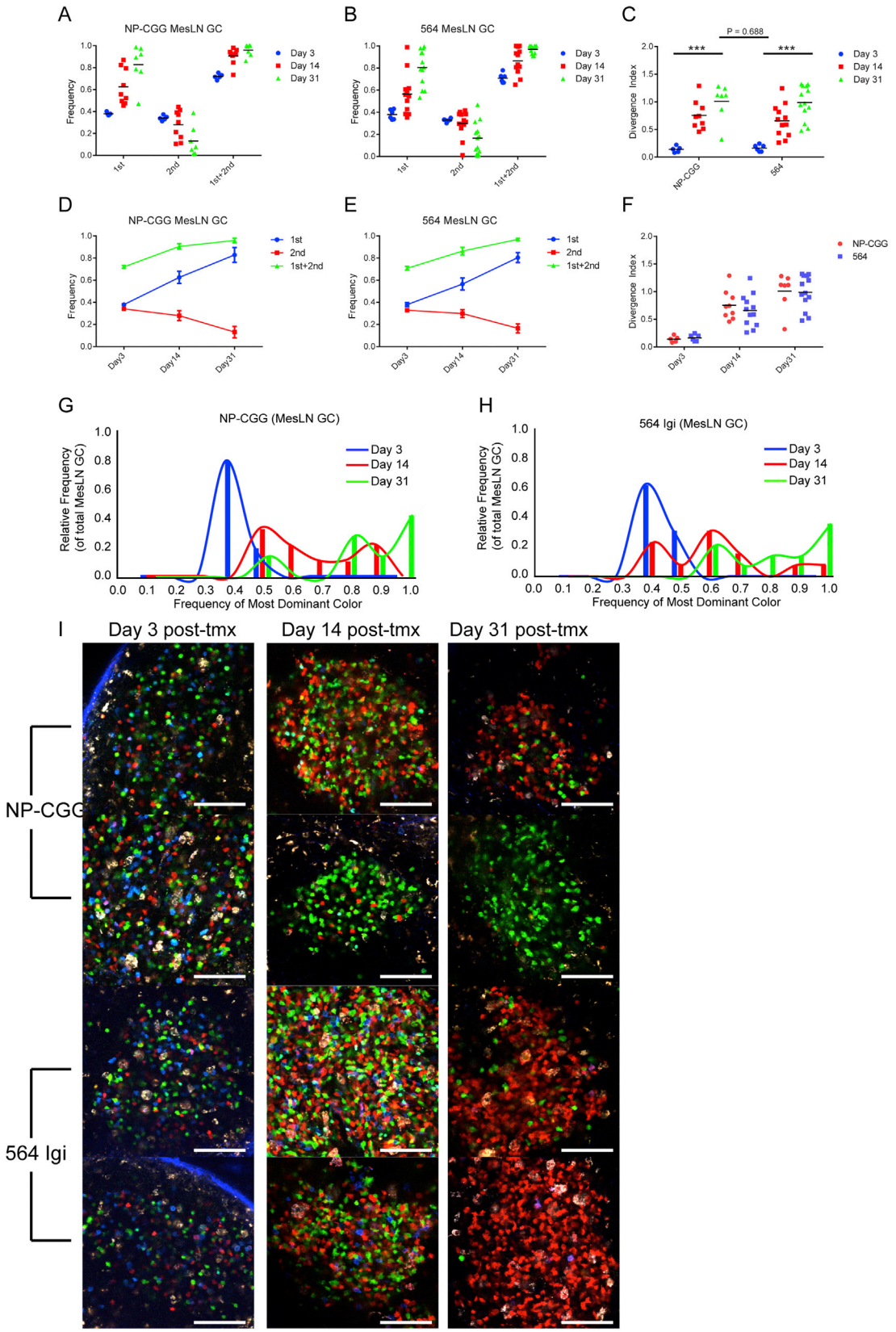

(legend on next page)

Figure S6. Clonal Evolution of Mesenteric GCs Followed in the Aid-Confetti Model, Related to Figure 5

(A) Frequency of most (1st), second most (2nd) and the sum of the most and second most predominant colors observed in individual mesenteric LN GC at Day 3, 14 and 31 post tamoxifen induction of Confetti recombination in NP-CGG immunized Confetti chimeras. The mean of an average of 3.7 GC per mouse in mesenteric LN of 2 mice per time point is indicated by the bar.

(B) As in (A), but for 564 Confetti mixed chimeras. The mean of an average of 3.7 GC per mouse in mesenteric LN of 3 mice per time point is indicated by the bar.

(C) Divergence index for the GC represented in (A) and (B). p values given for two-way ANOVA with Tukey's posttest (***$p < 0.001$).

(D) Line graph showing evolution of average frequencies of most, second most, and the sum of the most and second most predominant colors over time. Data as in (A).

(E) As in (D), but for 564 data as in (B).

(F) Divergence index data as in (C), but with a side-by-side comparison of NP-CGG and 564 chimeras at each time point.

(G) For NP-CGG immunized Confetti chimeras, the relative frequency of GC out of total mesenteric GC, plotted as a function of frequency of the most dominant color within each GC, demonstrating the shift over time from a high frequency of no-dominance GC (most dominant color = ~0.35) to a higher frequency of color-dominant GC (most dominant color frequency increases above 50%, i.e., 0.5, and beyond).

(H) as for (G), but for 564 Confetti mixed chimeras.

(I) Representative images used for quantification of color.

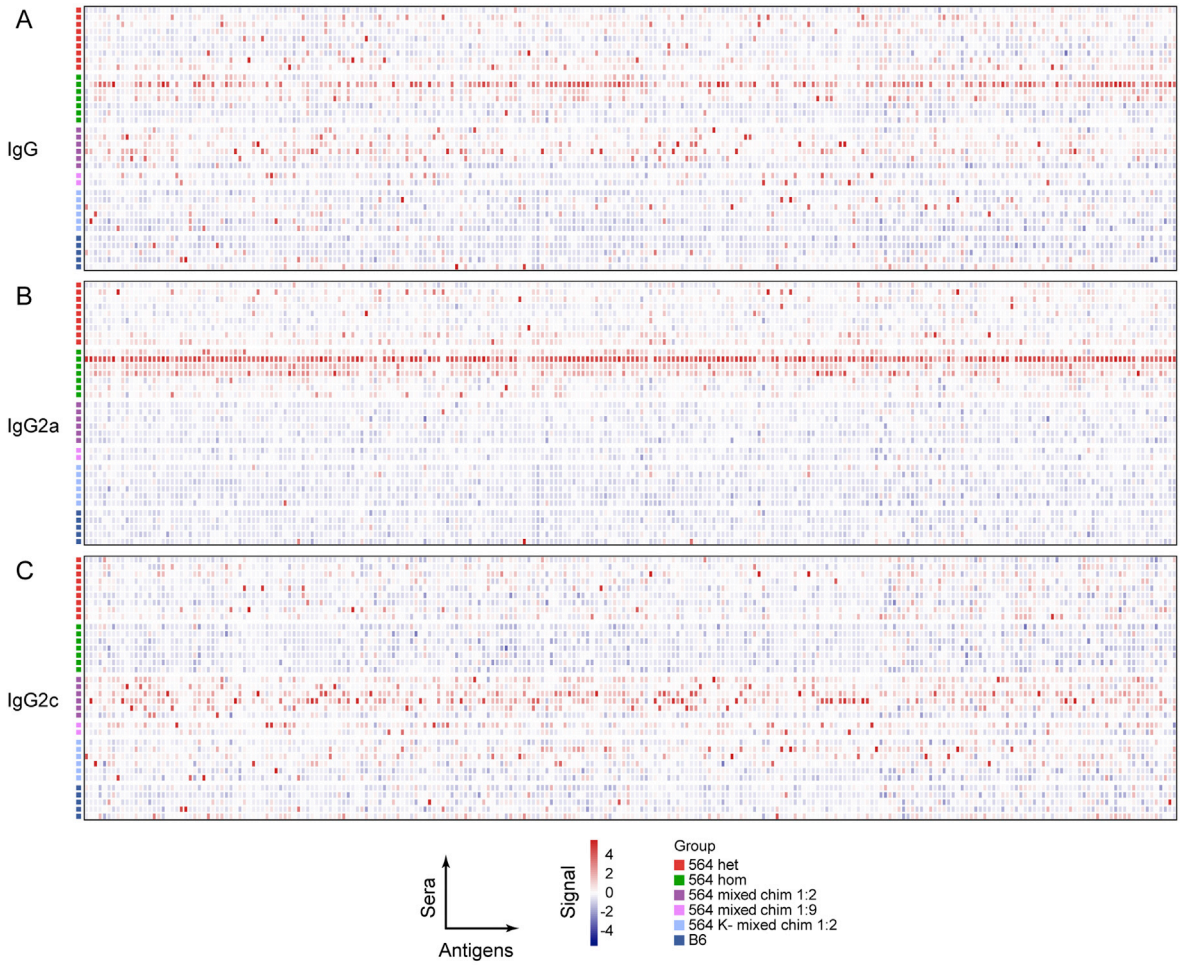

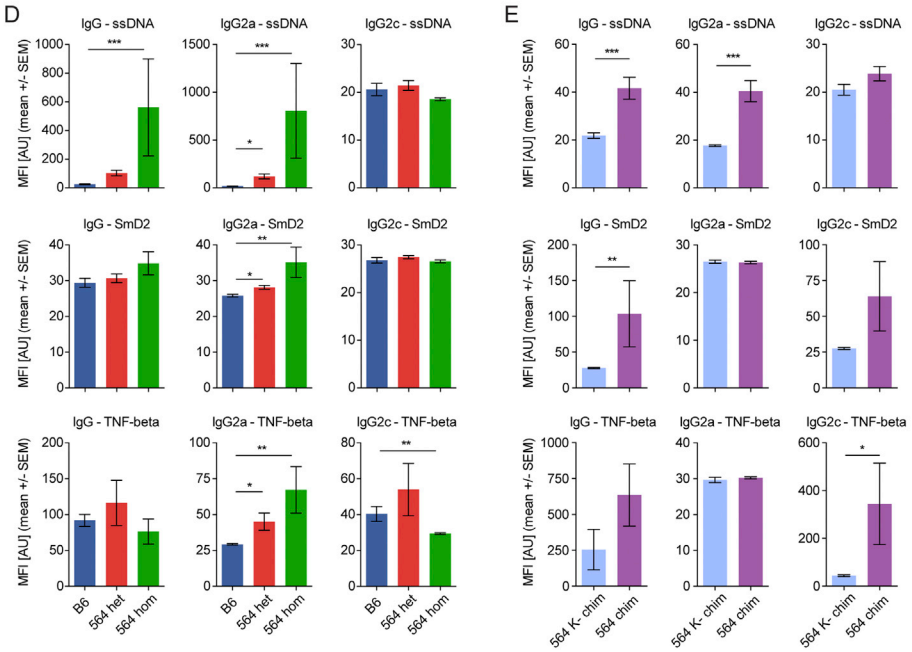

(legend on next page)

Figure S7. Autoantigen Array Profiling of Serum Antibodies, Related to Figure 6

(A) Overall patterns of reactivities of IgG in sera from 9 heterozygous 564Igi, 7 homozygous 564Igi, 6 1:2 564 mixed chimeras, 2 1:9 564 mixed chimeras, 6 1:2 564K- mixed chimeras, and 5 B6, assayed for 241 Ags. Each row represents a mouse, and mice are grouped as indicated in the legend. Each column represents an Ag (for a list of Ags in order left to right, please refer to Table S3). The log2-transformed signal intensity scale is indicated in the legend, going from high signal (red) to low signal (blue).

(B) As in (A), but for IgG2a development.

(C) As in (A), but for IgG2c development.

(D) Bar graph representations of IgG (left column), IgG2a (middle column) and IgG2c (right column) Ab toward single-stranded DNA (top row), SmD2 (middle row) and TNF-β (bottom row), in sera of B6 (n = 5), heterozygous (n = 9), and homozygous (n = 7) 564Igi mice. Mean ± SEM and multiplicity adjusted significance for one-way ANOVA with Dunn's posttest.

(E) Bar graph representations of IgG (left column), IgG2a (middle column) and IgG2c (right column) Ab toward single-stranded DNA (top row), SmD2 (middle row) and TNF-β (bottom row), in sera of 564 mixed chimeras (n = 8) and 564K- mixed chimeras (n = 6). Mean ± SEM and multiplicity adjusted significance for two-tailed Mann-Whitney test.